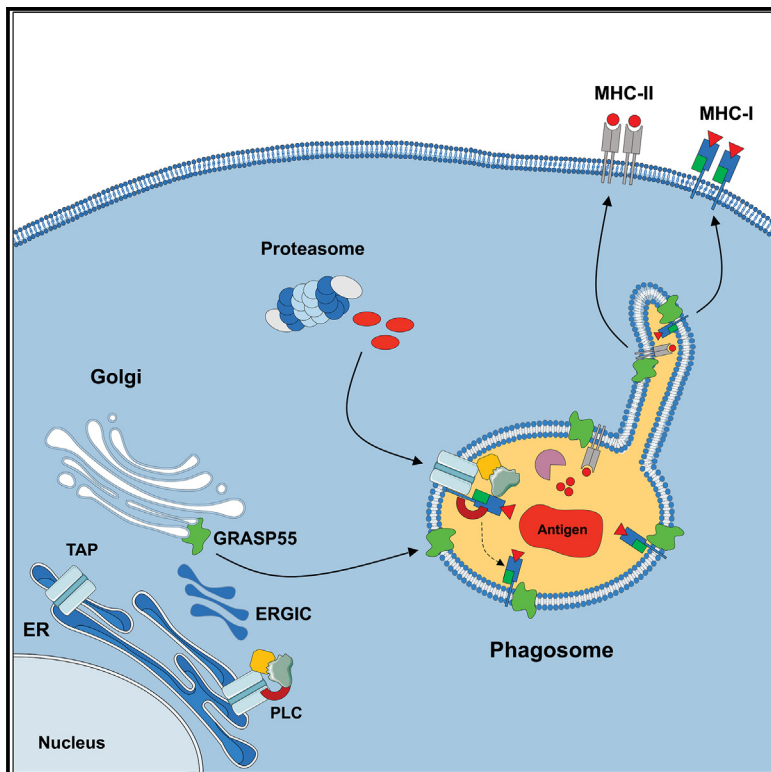


Dendritic cell phagosomes recruit GRASP55 for export of antigen-loaded MHC molecules

Graphical abstract



Authors

Ignacio Cebrian, Sofía Dinamarca, María Jesús Pena Rodríguez, ..., Nicolas Blanchard, David Sancho, Vivek Malhotra

Correspondence

icebrian@mendoza-conicet.gob.ar (I.C.), vivek.malhotra@crg.eu (V.M.)

In brief

Cebrian et al. demonstrate that the Golgi membrane-associated protein GRASP55 is recruited to late phagosomes in BMDCs. This interaction is essential for trafficking peptide-loaded MHC-I and MHC-II molecules to the cell surface and for achieving efficient exogenous antigen presentation by BMDCs.

Highlights

- GRASP55 is recruited to late BMDC phagosomes
- GRASP55 controls the phagosomal sorting of peptide-loaded MHC-I and MHC-II molecules
- GRASP55 regulates MHC-I cross-presentation and MHC-II antigen presentation by BMDCs



Article

Dendritic cell phagosomes recruit GRASP55 for export of antigen-loaded MHC molecules

Ignacio Cebrian,^{1,2,*} Sofía Dinamarca,^{1,2} María Jesús Pena Rodríguez,¹ Elena Priego,³ Nathalie Brouwers,¹ Martina Barends,⁴ Jamina Brunnberg,⁴ Robert Tampé,⁴ Nicolas Blanchard,⁵ David Sancho,³ and Vivek Malhotra^{1,6,*}

¹Centre for Genomic Regulation (CRG), The Barcelona Institute for Science and Technology, Dr. Aiguader 88, 08003 Barcelona, Spain

²Instituto de Histología y Embriología de Mendoza (IHEM)-CONICET, Facultad de Ciencias Médicas, Universidad Nacional de Cuyo, Mendoza 5500, Argentina

³Immunobiology Laboratory, Centro Nacional de Investigaciones Cardiovasculares (CNIC), Madrid, Spain

⁴Institute of Biochemistry, Biocenter, Goethe University Frankfurt, Max-von-Laue-Str. 9, 60438 Frankfurt am Main, Germany

⁵Toulouse Institute for Infectious and Inflammatory Diseases (Infinity), INSERM/CNRS/Université Toulouse 3, 31300 Toulouse, France

⁶Lead contact

*Correspondence: icebrian@mendoza-conicet.gob.ar (I.C.), vivek.malhotra@crg.eu (V.M.)

<https://doi.org/10.1016/j.celrep.2025.115333>

SUMMARY

Dendritic cells (DCs) present exogenous antigens via major histocompatibility complex class I (MHC-I) and MHC class II (MHC-II) molecules, activating CD8⁺ and CD4⁺ T cells. A critical but poorly understood step in this process is the trafficking of peptide-loaded MHC molecules from the endocytic system to the cell surface. In this study, we demonstrate that the Golgi reassembly-stacking protein of 55 kDa (GRASP55), which has been shown to have no role in stacking, is essential for antigen presentation. Using soluble, bead-coated, and bacterial-bound antigens, we found significantly impaired exogenous antigen presentation in GRASP55-deficient bone-marrow-derived DCs (BMDCs). Notably, GRASP55 was recruited to late phagosomes, and our data suggest that it is crucial for sorting MHC-I and MHC-II molecules, facilitating their trafficking to the plasma membrane. Our findings highlight the vital role of GRASP55 in the intracellular transport of MHC molecules bound to their respective peptides during exogenous antigen presentation.

INTRODUCTION

Dendritic cells (DCs) internalize exogenous antigens, such as pathogenic microbes or dying tumor cells, which are processed and displayed on the cell surface as peptides bound to major histocompatibility complex class II (MHC-II) molecules to activate CD4⁺ T lymphocytes. In another pathway, the exogenous-antigen-derived peptides are loaded onto MHC class I (MHC-I) molecules to activate CD8⁺ T cells.¹ Both pathways strongly rely on the endocytic network to generate peptides within endosomes or phagosomes depending on whether DCs internalize soluble or particulate antigens.²

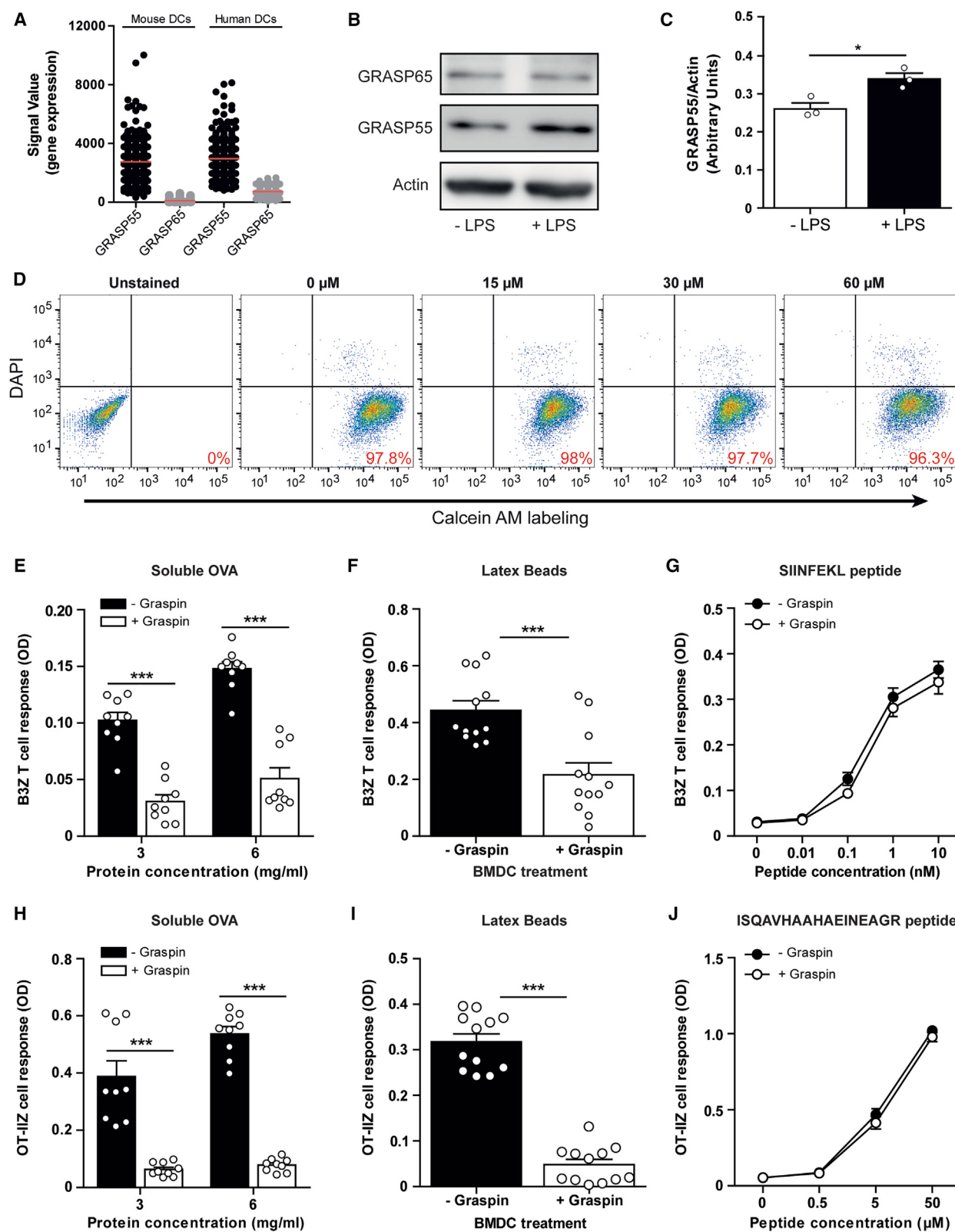
Phagosomes compose a key central compartment in the process of antigen processing. Phagosomes recruit vesicles carrying components from various compartments for the successful loading and presentation of the peptide-MHC complex (pMHC). This includes endoplasmic reticulum (ER)-Golgi intermediate compartment (ERGIC)-derived vesicles containing the peptide loading complex (PLC) and other relevant molecules.³ DC phagosomes also recruit recycling-compartment-derived vesicles, which represent the main source of MHC-I molecules.⁴ It is unclear whether MHC-II molecules reach the endocytic system via the Golgi apparatus⁵ or the plasma membrane.^{6,7} However, MHC-II molecules mostly accumulate within a late endosomal organelle known as the MHC-II-rich compartment (MIIC) that

meets the antigen-containing endosome/phagosome.⁸ Finally, lysosomes also fuse with phagosomal membranes to supply an acidic environment and proteases.⁹

This unique composition of DC phagosomes is reminiscent of the compartment for unconventional protein secretion (CUPS) in yeast. CUPS is composed of membranes derived from the Golgi and endosomes.^{10,11} The studied marker of CUPS is a protein called Golgi reassembly-stacking protein (GRASP), which is encoded by the *GRH1* gene in yeast.¹² Grh1 forms a complex with Bug1, a coiled-coil protein resembling metazoan GM130. Additionally, Grh1 interacts with the Sec23/24 proteins of the coat protein complex II.¹³ Mammalian cells contain two GRASP proteins, GRASP55 and GRASP65. Compared to GRASP65, GRASP55 is highly expressed in immune cells.^{14,15} GRASP55 regulates the activity of IRE1 α arm of the unfolded protein response pathway and the secretion of interleukin (IL)-1 β from activated macrophages.¹⁶ Interestingly, the known regulator of cross-presentation Sec22b also controls the unconventional secretion of IL-1 β .¹⁷

The similarities between phagosomes and CUPS and the intracellular logistics for exogenous antigen presentation and unconventional protein secretion pathways prompted us to test the involvement of GRASP55 in antigen presentation by DCs. We tested this by (1) use of a specific GRASP55 inhibitor called Graspin¹⁸ and (2) *GRASP55*^{-/-} bone-marrow-derived DCs





(legend on next page)

(BMDCs). In both cases, GRASP55 was found to be required for efficient presentation of exogenous antigens to CD4⁺ and CD8⁺ T cells. We show that GRASP55 is recruited to BMDC phagosomes at late time points post internalization and contributes to the sorting and trafficking of pMHC from phagosomes to the plasma membrane. However, GRASP55 does not have an obvious role in exogenous antigen presentation by tissue-resident DCs, endogenous antigen presentation, antigen uptake, or phagosomal maturation. Interestingly, we observed that GRASP55 is excluded from the *Toxoplasma gondii* parasitophorous vacuole (PV) and does not contribute to the presentation of *T. gondii*-derived antigens. In contrast, GRASP55 strongly intercepts *Escherichia coli*-containing phagosomes, and therefore the presentation of bacterium-associated antigens to CD4⁺ and CD8⁺ T cells is significantly impaired.

RESULTS

Graspin inhibits exogenous antigen presentation by DCs

We chose a bioinformatics tool called ImmCo, which presents means to evaluate co-expression and correlation between two given genes in a defined cell type of the mouse and human immune system.¹⁹ We noted that DCs in both mouse and human express GRASP55 at much higher levels compared to GRASP65 (Figure 1A). We differentiated BMDCs from C57BL/6 mice, and upon lipopolysaccharide (LPS) maturation, we observed a significant increase of GRASP55 but not GRASP65 expression (Figures 1B and 1C). We treated BMDCs and the JAWS-II DC line with a GRASP55 inhibitor called Graspin, which affects the stability and expression of GRASP55 by inhibiting PDZ-mediated interactions of GRASP55 with junctional adhesion molecule-C.¹⁸ Immunoblot analysis revealed that the treatment of BMDCs and JAWS-II DCs with Graspin downregulated GRASP55 expression in a dose-dependent manner (Figures S1A and S1B). The viability of these DC types, even at the highest concentration of Graspin, was unaffected, as shown by calcein AM staining and flow cytometry (Figures 1D and S1C).

To address the effect of Graspin treatment on antigen presentation, we first performed a dose-dependent cross-presentation response to Graspin in JAWS-II DCs. Graspin-treated and untreated cells were incubated with soluble ovalbumin (OVA) or 3-μm latex beads coated with OVA to measure the presentation of the antigen internalized by endocytosis or phagocytosis, respectively. After antigen uptake, DCs were fixed and exposed to B3Z CD8⁺ T cells. B3Z cells are activated upon recognition of

H-2K^b MHC-I molecules in association with the SIINFEKL peptide, which contains the amino acids 257–264 of OVA. We found that Graspin-treated JAWS-II DCs were impaired in antigen cross-presentation, and this effect correlated with increasing concentrations of Graspin (Figures S1D and S1E). In contrast, presentation of the SIINFEKL control peptide, which does not require intracellular processing, was not significantly affected by Graspin treatment (Figure S1F).

Compared to the classical BMDCs, JAWS-II DCs do not express high levels of MHC-II molecules.²⁰ Therefore, it is not possible to assess CD4⁺ T cell activation by JAWS-II cells. We therefore incubated BMDCs with 50 μM Graspin together with soluble OVA or OVA-coated 3-μm latex beads. In this experimental setup, we exposed Graspin-treated and untreated BMDCs to either B3Z or OT-IIZ T cells, which recognize a 17-amino-acid sequence (residues 323–339, peptide ISQAVHAAHAEINEAGR) in OVA bound to I-A^b MHC-II molecules.²¹ There was significant inhibition of MHC-I cross-presentation (Figures 1E and 1F) and MHC-II presentation (Figures 1H and 1I) by Graspin-treated BMDCs compared to untreated control cells. However, the presentation of the already processed control peptides showed similar levels of CD8⁺ and CD4⁺ T cell activation (Figures 1G and 1J). Because BMDC stimulation with LPS increases GRASP55 expression (Figures 1B and 1C) and can boost the ability to present exogenous antigens,^{8,22} we tested cross-presentation and MHC-II presentation in Graspin- and LPS-treated BMDCs. We found that the cross-presentation capacity of soluble OVA (Figure S1G) and OVA-coated 3-μm latex beads (Figure S1H) increased in both Graspin-treated and untreated BMDCs upon LPS stimulation. However, the CD8⁺ T cell response induced by Graspin-treated BMDCs remained significantly lower than the activation of B3Z cells exposed to BMDCs treated with LPS but without Graspin. Similar results were obtained by evaluating MHC-II presentation of OVA internalized by endocytosis (Figure S1I) or phagocytosis (Figure S1J).

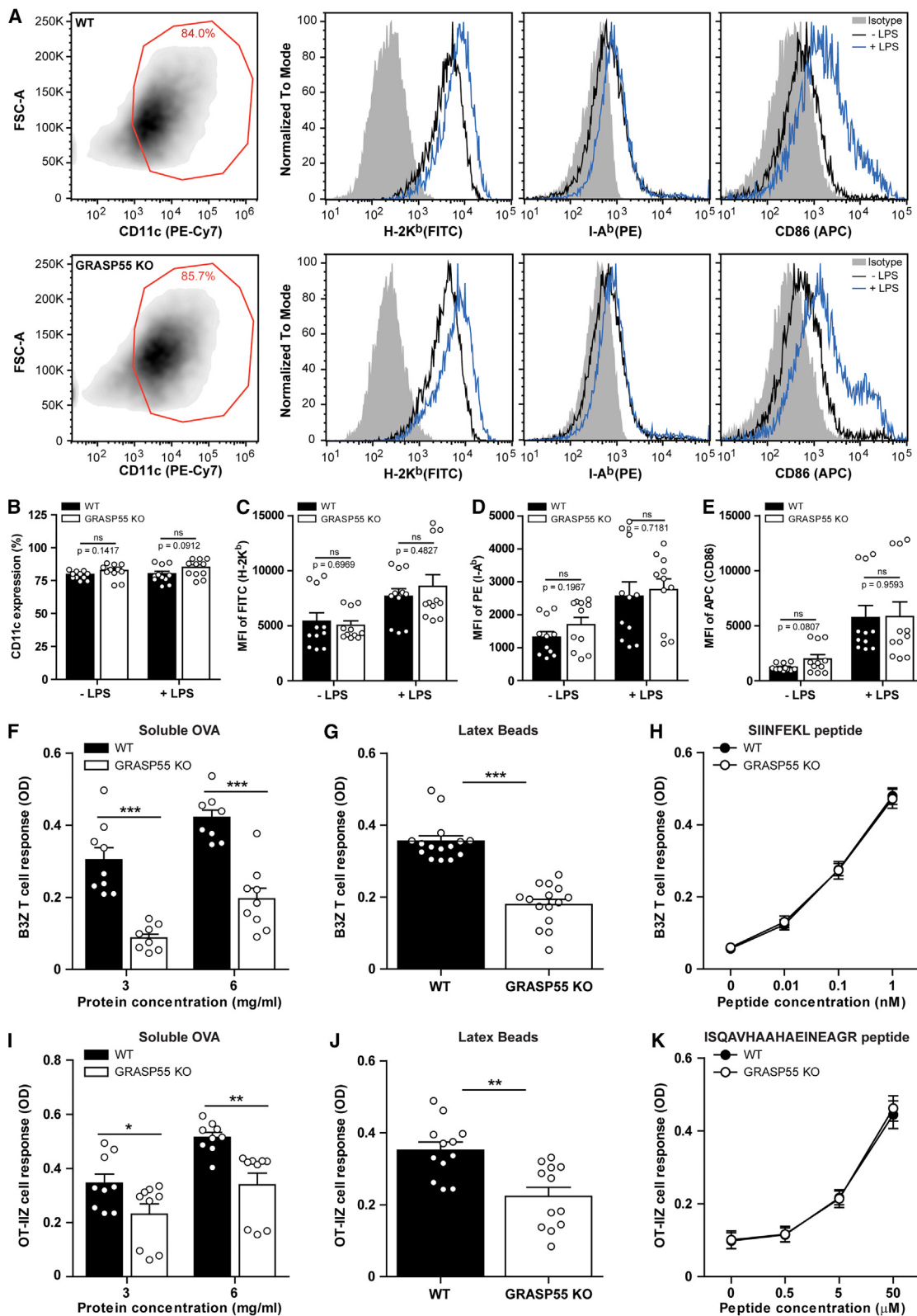
These data indicate that Graspin treatment affects intracellular processing and/or transport of soluble and particulate antigens during cross-presentation and MHC-II presentation without affecting the normal levels of MHC-I and -II molecules at the DC surface.

GRASP55^{-/-} BMDCs fail to present exogenous antigens to CD8⁺ and CD4⁺ T cells

To directly test the role of GRASP55 in exogenous antigen presentation, we used DCs from a mouse knockout for GRASP55.¹⁶

Figure 1. Graspin inhibits exogenous antigen presentation by BMDCs

- (A) *In silico* analysis showing the co-expression profiles of GRASP55 and GRASP65 by mouse and human DCs.
 - (B) Immunoblotting showing GRASP55, GRASP65, and actin expression by BMDCs left untreated or treated with LPS.
 - (C) Densitometry quantification of the GRASP55/actin ratio. Data show mean ± SEM of three independent experiments. *p = 0.0231.
 - (D) FACS analysis showing DAPI and calcein AM labeling of BMDCs left untreated or treated with increasing concentrations of Graspin. The lower right quadrants show the percentages of viable cells. Data are representative of triplicate values from 3 independent experiments.
 - (E–G) The MHC-I cross-presentation ability of Graspin-treated and untreated BMDCs was evaluated after incubation with (E) soluble OVA, (F) OVA-coated 3-μm beads, and (G) the SIINFEKL peptide. Data represent mean ± SEM of triplicate values from (E) 3 or (F and G) 4 independent experiments. (E) ***p < 0.0001 and (F) ***p = 0.0004.
 - (H–J) The MHC-II antigen presentation ability of Graspin-treated and untreated BMDCs was evaluated after incubation with (H) soluble OVA, (I) OVA-coated 3-μm latex beads, and (J) the ISQAVHAAHAEINEAGR peptide. Data represent mean ± SEM of triplicate values from (H) 3 or (I and J) 4 independent experiments. ***p < 0.0001.
- Unpaired two-tailed Student's t test was performed. See also Figure S1.



(legend on next page)

We differentiated BMDCs from wild-type (WT) and *GRASP55*^{-/-} mice. The expression of the classical DC marker CD11c was greater than 80% in both types of DCs (Figures 2A and 2B), and we did not observe any significant difference in the cell surface expression of MHC-I H-2K^b and MHC-II I-A^b molecules with or without LPS treatment (Figures 2A, 2C, and 2D). Also, DC maturation was not impaired in *GRASP55*^{-/-} BMDCs, as CD86 expression was upregulated upon LPS treatment at similar levels compared to WT BMDCs (Figures 2A and 2E). We also investigated the expression profile of the maturation marker CD83 because it has been described as an interaction partner of GRASP55 in human DCs. In these cells, The C-terminal TELV motif of CD83 binds to GRASP55, and this interaction leads to efficient CD83 glycosylation and cell surface expression.²³ As shown in Figures S2A and 2B, we did not find any defect of CD83 expression in *GRASP55*^{-/-} BMDCs. On the contrary, the cell surface expression of CD83 was higher in *GRASP55*^{-/-} BMDCs upon LPS stimulation as compared to WT BMDCs.

Following the characterization of WT and *GRASP55*^{-/-} BMDC phenotypes, we tested their ability to present exogenous antigens. We used soluble and particulate OVA to test MHC-I cross-presentation and MHC-II presentation. CD8⁺ T cell activation was significantly reduced by *GRASP55*^{-/-} BMDCs exposed to B3Z cells compared with WT BMDCs (Figures 2F and 2G). Similar results were obtained by analyzing the activation of OT-IIZ CD4⁺ T cells (Figures 2I and 2J). However, the presentation of the short control OVA peptides 357–264 and 323–339 to B3Z and OT-IIZ cells, respectively, showed no significant differences between WT and *GRASP55*^{-/-} BMDCs (Figures 2H and 2K). Similar to our approach with Graspin-treated BMDCs, we evaluated the exogenous antigen presentation capacity of *GRASP55*^{-/-} BMDCs in the context of LPS treatment. Also, in this experimental setup, we found that *GRASP55*^{-/-} BMDCs increased both MHC-I cross-presentation and MHC-II presentation abilities for soluble (Figures S2C and S2E) and particulate OVA (Figures S2D and 2F) upon LPS stimulation. However, for all cases, T cell activation induced by *GRASP55*^{-/-} LPS-treated BMDCs was significantly lower than in their WT LPS-treated counterparts. We next aimed to control the specificity of Graspin by treating WT and *GRASP55*^{-/-} BMDCs with this inhibitor and performed exogenous antigen presentation assays. For MHC-I cross-presentation of both soluble and particulate OVA, we evidenced that this drug showed correct specificity, and *GRASP55*^{-/-} untreated and Graspin-treated BMDCs did not exhibit significant differences of CD8⁺ T cell activation (Figures S2G and S2H). However, for MHC-II antigen presentation, the scenario was different. In this case, *GRASP55*^{-/-}

Graspin-treated BMDCs further inhibited CD4⁺ T cell response (Figures S2I and S2J), suggesting that BMDC treatment with Graspin most likely affects other critical molecules of the MHC-II antigen presentation pathway.

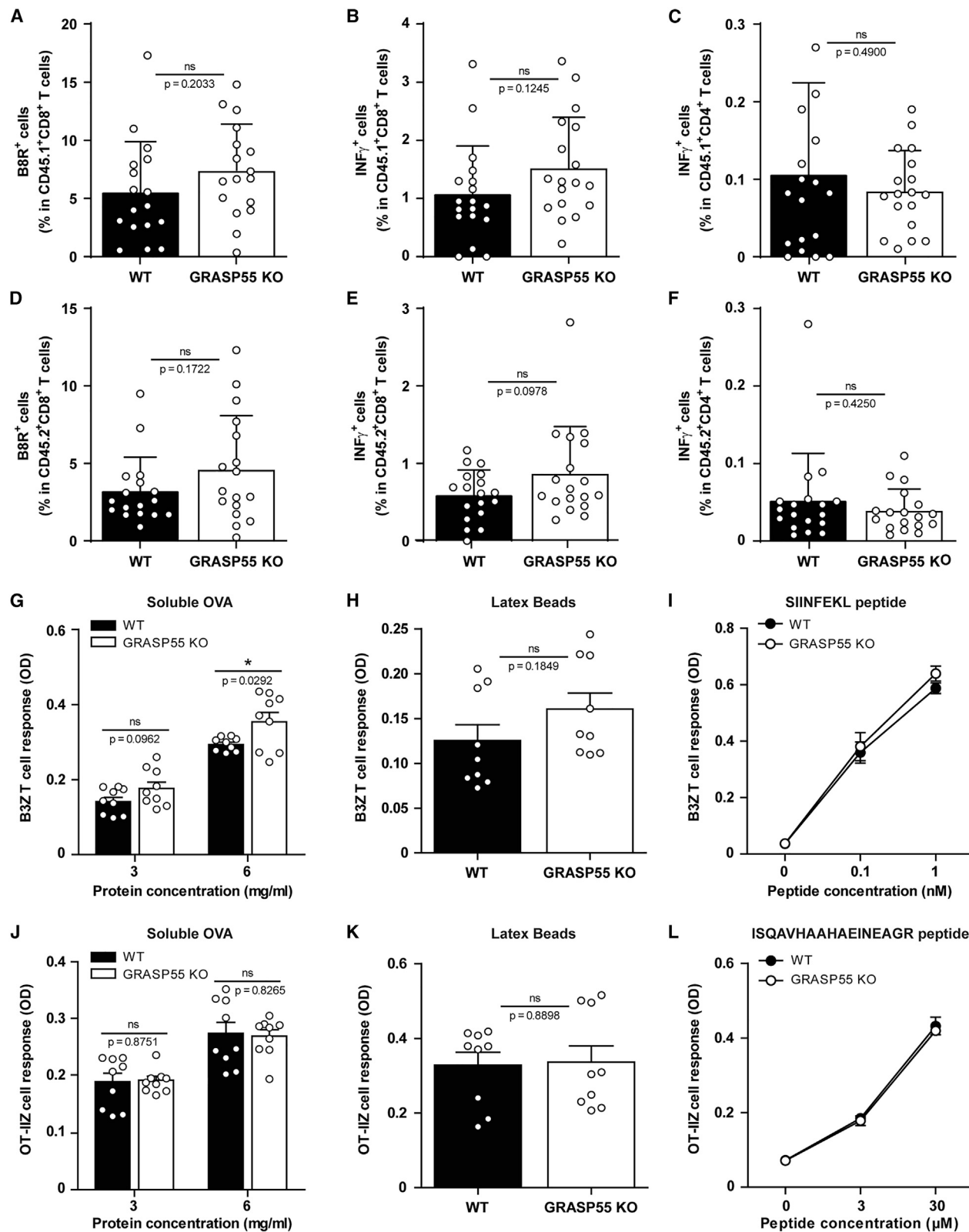
Finally, we tested the relevance of GRASP55 in tissue-resident DCs by two different experimental approaches: (1) *in vivo* exogenous antigen presentation using chimera WT and *GRASP55*^{-/-} mice and (2) *in vitro* exogenous antigen presentation using splenic DCs isolated from WT and *GRASP55*^{-/-} mice. For the first set of experiments, we generated the chimera mice and injected them intraperitoneally with vaccinia virus expressing OVA (VACV-OVA)-infected RAW macrophages treated with UV light to inactivate the virus. In this way, we block direct infection of DCs and leave available only the exogenous antigen presentation routes.²⁴ After 1 week of injection, splenic cells were collected and divided for (1) flow cytometry analysis (percentage of B8R⁺ cells), (2) 2-h culture in presence of B8R peptide 20–27, and (3) an overnight (ON) culture in presence of the OVA peptides 262–276 and 323–339. After each of these cultures, cells were treated with brefeldin A, fixed, and stained for fluorescence-activated cell sorting (FACS) analyses. We checked the chimera's reconstitution by flow cytometry and found that nearly 100% of CD45.2⁺ neutrophils were present in the blood, confirming full DC reconstitution in these mice (Figure S3A). On the other hand, T cell composition in the spleen held between 10% and 50% of CD45.1⁺ resident CD8⁺ and CD4⁺ T cells (Figures S3B and S3C, respectively). This allows studying the effects of the assay, not only in donor CD45.2⁺ T cells but also in resident CD45.1⁺ T cells from the same WT genotype within the same chimera mouse. Specific CD8⁺ T cell response to B8R antigen from VACV in the spleen showed no significant differences between WT and *GRASP55*^{-/-} DCs, either by analyzing CD45.1⁺ resident or CD45.2⁺ donor T cells (Figures 3A and 3D, respectively). We also measured CD8⁺ T cell response by detecting interferon (IFN γ) production upon restimulation with the B8R peptide, obtaining similar results (Figures 3B and 3E). To evaluate MHC-II antigen presentation, we analyzed the percentage of IFN γ producing CD4⁺ T cells upon restimulation with the OVA peptides. Again, we did not find significant differences of CD4⁺ T cell response between WT and *GRASP55*^{-/-} DCs (Figures 3C and 3F).

We also isolated splenic DCs from WT and *GRASP55*^{-/-} mice and incubated them with soluble OVA, OVA-coated 3- μ m latex beads or the short control OVA peptides, residues 257–264 and 323–339. Then, DCs were fixed and exposed to B3Z or OT-IIZ cells. In this experimental setup, we did not evidence defective MHC-I cross-presentation (Figures 3G–3I) or MHC-II antigen

Figure 2. *GRASP55* controls the presentation of exogenous antigens to CD8⁺ and CD4⁺ T cells by BMDCs

(A–E) WT and *GRASP55*^{-/-} LPS-treated and untreated BMDCs were labeled for CD11c, H-2K^b, I-A^b, and CD86 and were analyzed by FACS. In (A), gates on CD11c-positive cells (red) are depicted on the left, and representative histograms showing the fluorescence intensity of H-2K^b, I-A^b, and CD86 in CD11c⁺ cells are depicted on the right. (B–E) Bars show the quantification of (B) CD11c⁺ cells and the MFI of (C) H-2K^b, (D) I-A^b, and (E) CD86 for each experimental condition. Data represent mean \pm SEM of triplicate values from 4 independent experiments (11 replicates, 1 experiment was done in duplicates). (F–H) The MHC-I cross-presentation ability of WT and *GRASP55*^{-/-} BMDCs was evaluated after incubation with (F) soluble OVA, (G) OVA-coated 3- μ m beads, and (H) the SIINFEKL peptide. Data represent mean \pm SEM of triplicate values from (F) 3, (G) 5, or (H) 7 independent experiments. *** p < 0.0001. (I–K) The MHC-II antigen presentation ability of WT and *GRASP55*^{-/-} BMDCs was evaluated after incubation with (I) soluble OVA, (J) OVA-coated 3- μ m latex beads, and (K) the ISQAVHAAHAEINEAGR peptide. Data represent mean \pm SEM of triplicate values from (I) 3, (J) 4, or (K) 5 independent experiments. (I) * p = 0.0389 and ** p = 0.0019, and (J) ** p = 0.0011.

Unpaired two-tailed Student's t test was performed. See also Figure S2.



(legend on next page)

presentation (Figures 3J–3L) by *GRASP55*^{−/−} splenic DCs as compared to their WT counterparts. To find a possible explanation for this discrepancy in the antigen presentation capacity of WT and *GRASP55*^{−/−} BMDCs and splenic DCs, we performed immunoblotting and were not able to detect any clear band corresponding to GRASP55 in splenic DCs (Figure S3D), suggesting very low expression of GRASP55 in these cells. Although GRASP55 protein expression could not be detected by immunoblotting in splenic DCs, we assessed GRASP55 mRNA expression levels by qPCR under different experimental conditions. We incubated total splenic DCs isolated from WT mice with 50 μM Graspin, 100 ng/mL *E. coli*-derived ultrapure LPS (to stimulate TLR4), or 5 μM class B CpG (to stimulate TLR9) or left them untreated. As expected, GRASP55 expression was notably reduced in Graspin-treated splenic DCs but increased significantly under LPS and CpG treatments, the two inflammatory environments tested (Figure S3E). These findings highlight the major relevance of GRASP55 under stressful conditions.

These data confirm the requirement of GRASP55 for exogenous antigen presentation in the MHC-I and -II pathways by BMDCs (inflammatory DCs) specifically but not by tissue-resident DCs.

GRASP55 does not regulate endogenous antigen presentation via MHC-I

Based on *in vitro* analyses, GRASP55 has been linked to laterally holding stacks of cisternae to compose a Golgi ribbon.²⁵ We therefore tested whether defects in overall Golgi organization were visible and could affect endogenous MHC-I antigen presentation in the *GRASP55*^{−/−} cells. We electroporated WT and *GRASP55*^{−/−} BMDCs with soluble OVA. In this setup, the antigen is directly introduced into the cytosol, and OVA peptides are loaded onto H₂K^b MHC-I molecules after transport in the ER lumen. The pMHC-I molecules transit through the classical secretory pathway to reach the plasma membrane. Figure 4A shows that WT and *GRASP55*^{−/−} BMDCs present endogenous antigens to CD8⁺ B3Z cells with similar efficiency. A higher trend of endogenous presentation was observed in *GRASP55*^{−/−} BMDCs compared to WT BMDCs, but overall, these differences were not statistically significant. Brefeldin A treatment, which inhibits the conventional ER-Golgi traffic, efficiently blocked MHC-I endogenous presentation (Figure 4A). Furthermore, the amount of OVA incorporated in WT and *GRASP55*^{−/−} BMDCs after electroporation was similar in both cell types (Figure 4B).

In addition to testing the functionality of the ER-to-Golgi transport in *GRASP55*^{−/−} BMDCs, we further examined the

morphology of the classical secretory pathway by immunostaining and confocal microscopy. Figures 4C–4F show that Protein disulfide isomerase (PDI, an ER marker), GM130 (a *cis* Golgi marker), TGN46 (a *trans* Golgi marker), and TGN38 (a *trans*-Golgi network marker) exhibit comparable labeling in WT and *GRASP55*^{−/−} BMDCs. Importantly, the intracellular distribution of H₂K^b molecules and ERGIC are similar in WT and *GRASP55*^{−/−} BMDCs (Figure S4). These data show that the overall Golgi organization and function in trafficking of MHC-I molecules internally loaded with an antigen are not affected in *GRASP55*^{−/−} BMDCs.

Altogether, GRASP55 is critical for exogenous antigen presentation in BMDCs but not for endogenous antigen presentation via MHC-I.

GRASP55 controls the transport of OVA-loaded MHC molecules from DC phagosomes to the plasma membrane

It is known that phagosome-to-plasma membrane transport is a key step in both MHC-I and MHC-II molecule presentation; we tested whether this step was affected in *GRASP55*^{−/−} DCs. We incubated both types of DCs with 3-μm magnetic particles for different periods. The phagosomes from WT and *GRASP55*^{−/−} BMDCs were isolated and immunoblotted with anti-GRASP55 and anti-Lamp1 antibodies. We observed the recruitment of GRASP55 only at late time points post internalization of the magnetic particles (3 and 5 h; Figure 5A). This result suggests that GRASP55 likely has an important role in the final steps of exogenous antigen presentation, such as the transport of pMHC molecules from phagosomes to the cell surface. To test this, we visualized WT and *GRASP55*^{−/−} BMDCs previously incubated with 3-μm OVA-coated latex beads for up to 5 h. We labeled these cells with the 25.D1 antibody, which recognizes H₂K^b MHC-I molecules in association with the SIINFEKL peptide. Clear 25.D1 labeling around the internalized beads that are also positive for Lamp1 was observed in WT cells, but interestingly, the labeling was stronger in *GRASP55*^{−/−} BMDCs (Figure 5B). To quantify these data, we performed flow cytometry experiments of phagosomes isolated from WT and *GRASP55*^{−/−} BMDCs at different time points post internalization of 3-μm OVA-coated latex beads. The results of this assay showed that the kinetics of 25.D1 labeling is different between WT and *GRASP55*^{−/−} phagosomes. While the presence of OVA/MHC-I complexes in WT phagosomes decreases at 5 h post internalization, these complexes accumulate in *GRASP55*^{−/−} phagosomes (Figures 5C and 5D).

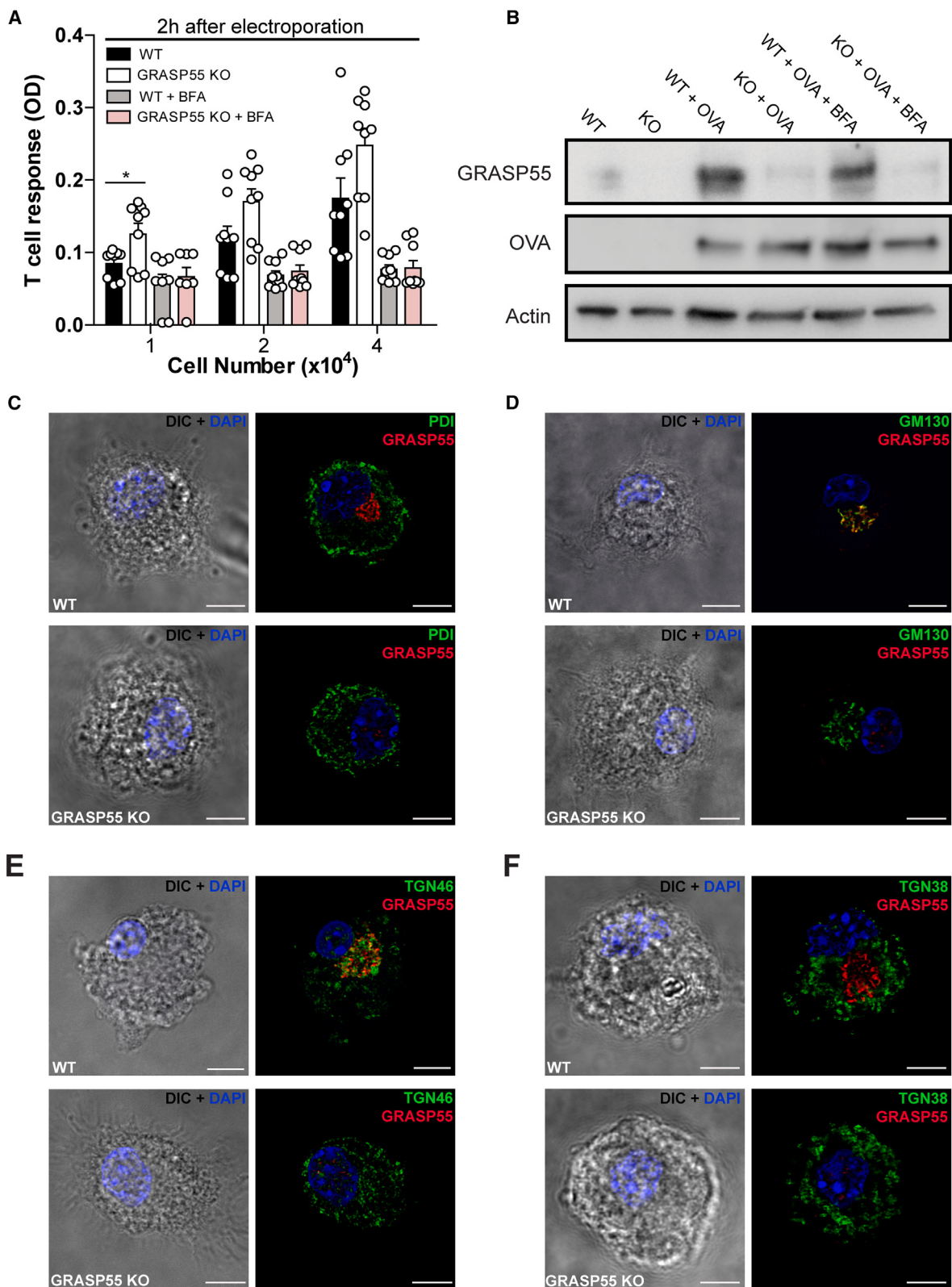
Figure 3. Exogenous antigen presentation by splenic DCs is independent of GRASP55

(A–F) B6/SJL CD45.1⁺ recipient mice were reconstituted with bone marrow precursors from C57BL/6 CD45.2⁺ WT or *GRASP55*^{−/−} mice. RAW macrophages infected with VACV-OVA and UV irradiated were inoculated intraperitoneally into chimeric mice. Cells were recovered by intraperitoneal lavage, and the number of B8R-specific (A) CD45.1⁺ (resident) and (D) CD45.2⁺ (donor) CD8⁺ T cells was measured using a fluorescently labeled MHC-I H₂K^b/B8R_{20–27} tetramer. IFN γ response in (B) CD45.1⁺ (resident) and (E) CD45.2⁺ (donor) CD8⁺ T cells after restimulation with B8R peptide, and IFN γ response in (C) CD45.1⁺ (resident) and (F) CD45.2⁺ (donor) CD4⁺ T cells after restimulation with the OVA peptides 323–339 and 262–276 was evaluated. Data show mean ± SEM of values from a pool of 2 independent experiments ($n = 9$ biological replicates for each experiment).

(G–I) The MHC-I cross-presentation ability of WT and *GRASP55*^{−/−} splenic DCs was evaluated after incubation with (G) soluble OVA, (H) OVA-coated 3-μm beads, and (I) the SIINFEKL peptide. Data represent mean ± SEM of triplicate values from 3 independent experiments.

(J–L) The MHC-II antigen presentation ability of WT and *GRASP55*^{−/−} splenic DCs was evaluated after incubation with (J) soluble OVA, (K) OVA-coated 3-μm latex beads, and (L) the ISQAVHAAHAEINEAGR peptide. Data represent mean ± SEM of triplicate values from 3 independent experiments.

Unpaired two-tailed Student's *t* test was performed. See also Figure S3.



(legend on next page)

To avoid any potential issue with the use of the 25.D1 antibody, we designed a different experimental procedure to investigate this transport event for both MHC-I and -II molecules. First, we coated 3- μ m magnetic beads with OVA, as confirmed by immunofluorescence staining and confocal microscopy (Figure S5A). We incubated WT and *GRASP55*^{-/-} BMDCs with OVA-coated magnetic particles for 1 and 5 h. We isolated the magnetic bead-containing phagosomes, fixed them, and disrupted the phagosomal membrane to expose OVA/MHC-I and -II complexes. Finally, we incubated these phagosomal fractions with CD8⁺ B3Z and CD4⁺ OT-II T cells. Interestingly, 1-h phagosomes isolated from WT and *GRASP55*^{-/-} BMDCs displayed similar abilities to activate B3Z and OT-II T cells. In contrast, 5-h phagosomes purified from *GRASP55*^{-/-} BMDCs showed greater capacity to activate both B3Z and OT-II T cells as compared to 5-h WT phagosomes (Figures 5E and 5F, respectively). This difference is also evident when we represent only the accumulation of OVA-loaded MHC-I and -II molecules at 5 h post internalization by subtracting the optical density of T cell activation at 1 h post internalization (Figures S5B and S5C).

Altogether, these data show that GRASP55 is recruited to DC phagosomes late in the maturation process and functions at this compartment to regulate the export of pMHC-I and pMHC-II for traffic to the cell surface.

GRASP55 is not required for antigen internalization or phagosomal maturation

Is GRASP55 involved in the internalization of exogenous antigens and phagosomal maturation? We evaluated fluid-phase endocytosis by flow cytometry after incubation of DCs with a fluorescently tagged OVA. Both WT and *GRASP55*^{-/-} BMDCs endocytose the antigen with similar efficiencies (Figures 6A and 6B). To evaluate phagocytosis, we coated 3- μ m latex beads with fluorescent OVA and incubated WT and *GRASP55*^{-/-} BMDCs with these particles. After uptake, cells were washed, fixed, and stained with an anti-OVA antibody to exclude by flow cytometry the plasma membrane-associated particles from those that are fully internalized (Figure 6C, lower right quadrants). The phagocytic capacities of WT and *GRASP55*^{-/-} BMDCs do not reveal any significant difference (Figures 6C and 6D).

To address the potential role of GRASP55 in phagosome maturation, WT and *GRASP55*^{-/-} BMDCs were incubated with 3- μ m OVA-coated latex beads for different times. Cells were then homogenized and phagosomes isolated by the established procedures.²⁶ The membrane fractions enriched in phagosomes were stained with anti-OVA and anti-Lamp1 antibodies

and analyzed by flow cytometry. OVA degradation in phagosomes was similar in both cell types (Figures 6E and 6F). In addition, the lysosomal marker Lamp1 was recruited to WT and *GRASP55*^{-/-} BMDC phagosomes at similar levels (Figures 6G and 6H).

A special property of cross-presentation is the endosome/phagosome-to-cytosol transport step of the internalized antigen. To investigate whether GRASP55 is involved in antigen translocation from endosomes to the cytosol, we used a flow cytometry-based approach after cytochrome c internalization that was originally described by others.^{3,27,28} Briefly, when cytochrome c is exported from endosomes to the cytosol, it binds Apaf-1 and activates a caspase cascade that leads to cell death. This form of apoptosis can be quantified by annexin V staining of untreated and cytochrome c-treated DCs by flow cytometry. The percentages of annexin V⁺ cells were similar for WT and *GRASP55*^{-/-} BMDCs with or without cytochrome c treatment (Figure S6A, lower right quadrants). Moreover, the mean fluorescence intensity (MFI) of these cells did not show significant differences in annexin V staining (Figure S6B).

Altogether, these data show that GRASP55 does not regulate antigen uptake (endocytosis and phagocytosis), phagosomal maturation, or endosome-to-cytosol antigen transport in BMDCs.

GRASP55 is recruited to *E. coli*-containing phagosomes to regulate antigen presentation

To assess the importance of GRASP55 during the presentation of microbe-associated antigens by BMDCs, we used two different antigenic models. First, we used *T. gondii*, an intracellular obligate parasite that induces strong CD8⁺ and CD4⁺ T cell responses. This parasite enters DCs by a parasite-driven active process, and the PV establishes tightly regulated connections with different intracellular DC compartments.²⁹ Second, we used *E. coli*, a gram-negative bacterium that enters DCs by regular phagocytosis, and the process of phagosomal maturation follows similar kinetics as we observe with inert particles (latex or magnetic beads).

Interestingly, we found that the presentation of two distinct *T. gondii*-derived antigens does not depend on GRASP55. To evaluate MHC-I presentation, we used the type I TgRH *GRA6-SL8* strain that expresses the OVA SIINFEKL peptide fused with the immunodominant, PV membrane-bound antigen *GRA6*.^{30,31} For MHC-II presentation, we used the TgRH yellow fluorescent protein (YFP)/SAG1-OVA strain, where the OVA model antigen is fused to the SAG1 protein and released as a soluble protein in the vacuole. After 12 h of infection, BMDCs were fixed and exposed to B3Z and OT-II T cells. There were no significant

Figure 4. GRASP55 does not regulate ER-Golgi transport or morphology in BMDCs

(A) Soluble OVA was electroporated into the cytosol of WT and *GRASP55*^{-/-} BMDCs, and CD8⁺ B3Z T cell activation was determined 2 h later. Brefeldin A (BFA) was used to control the specificity of endogenous MHC-I antigen presentation. Data represent mean \pm SEM of triplicate values from 3 independent experiments. *p = 0.0230. Unpaired two-tailed Student's t test was performed.

(B) Immunoblot showing the amount of OVA incorporated by WT and *GRASP55*^{-/-} BMDCs after OVA electroporation and BFA treatment.

(C–F) Confocal microscopy analysis showing the localization of endogenous GRASP55 (red) and different markers of the classical secretory pathway (green) in WT and *GRASP55*^{-/-} BMDCs: (C) the ER marker PDI, (D) the *cis* Golgi marker GM130, (E) the *trans*-Golgi marker TGN46, and (F) the *trans*-Golgi network marker TGN38. The nuclear marker DAPI (blue) and differential interference contrast (DIC) images are shown on the left. Overlays of all fluorescent channels are shown on the right. Scale bars: 5 μ m.

Data are representative of at least 30 images analyzed for each marker from 3 independent experiments. See also Figure S4.

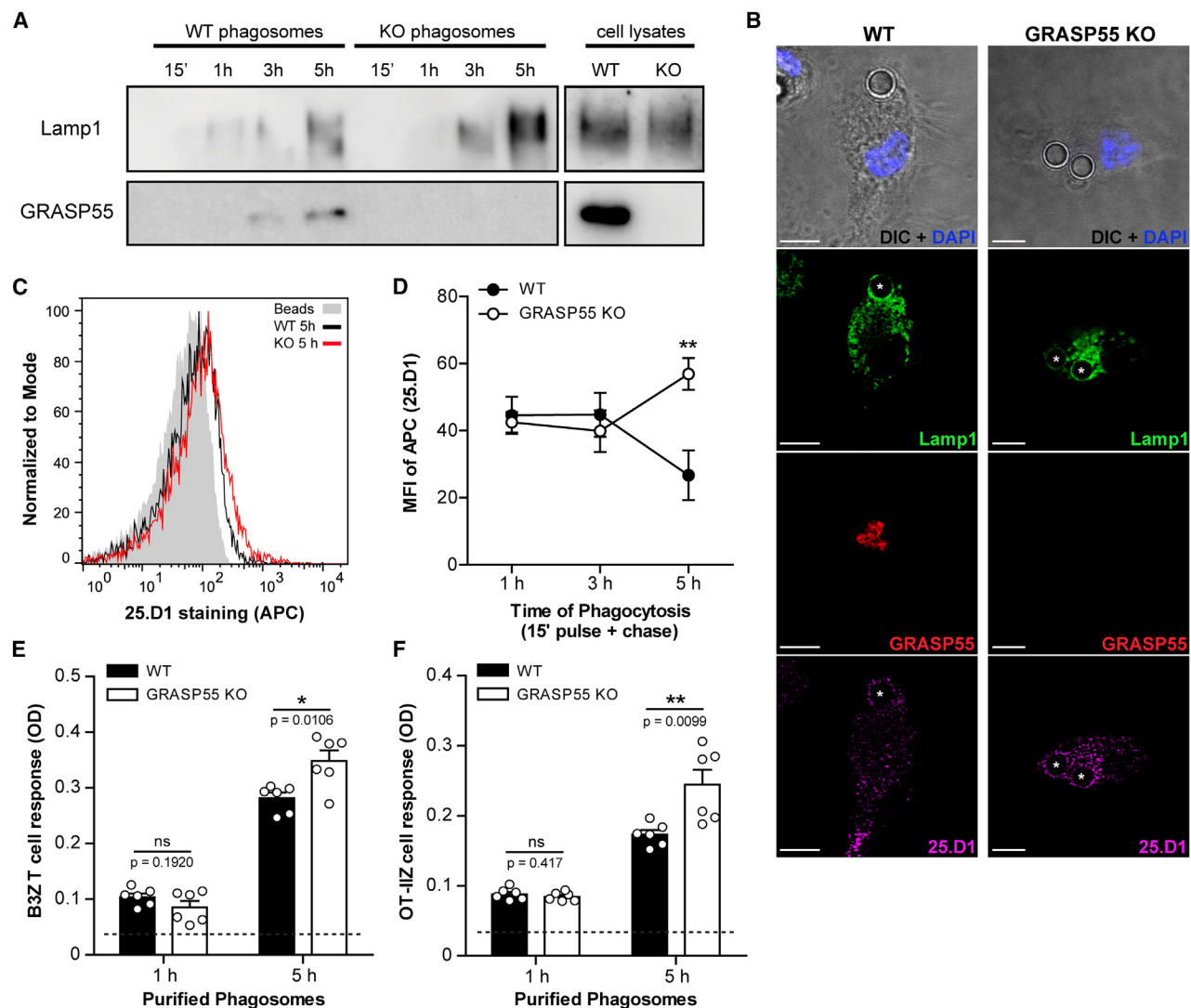


Figure 5. Phagosomal recruitment of GRASP55 and transport of OVA-loaded MHC molecules to the plasma membrane in BMDCs

(A) Immunoblot of WT and *GRASP55*^{-/-} BMDC purified phagosomes and total cell lysates showing the detection of Lamp1 and GRASP55. The blot is representative of 3 independent experiments.

(B) Immunofluorescence labeling and confocal microscopy analysis showing the detection of Lamp1 (green), GRASP55 (red), and SIINFEKL-loaded MHC-I H-2K^b molecules (25.D1, magenta) in WT and *GRASP55*^{-/-} BMDCs incubated with 3-μm OVA-coated latex beads for 5 h. Nuclei stained with DAPI and DIC images are shown at the top. White asterisks indicate the latex beads. Scale bars: 5 μm. Data are representative of at least 30 images analyzed from 3 independent experiments.

(C) Representative FACS profiles of 25.D1 staining on isolated phagosomes after 5 h of OVA-coated 3-μm latex bead internalization by WT (black line) and *GRASP55*^{-/-} (red line) BMDCs. Non-internalized latex beads representing the background staining are shown in gray.

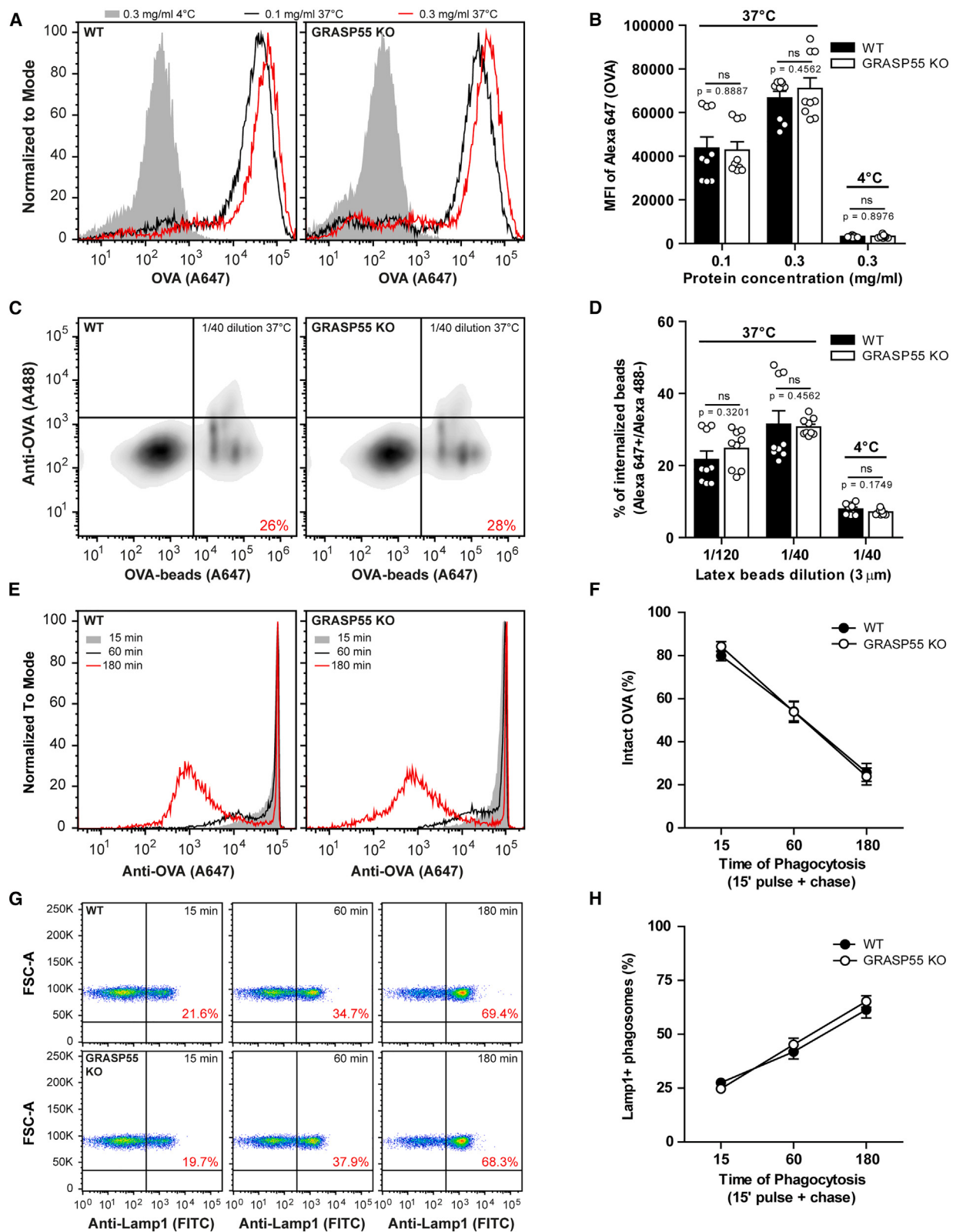
(D) FACS analysis and quantification of 25.D1 staining on WT and *GRASP55*^{-/-} BMDC isolated phagosomes. Data represent mean ± SEM of triplicate values from 3 independent experiments. **p < 0.01. A two-way ANOVA and Bonferroni post-test were performed.

(E and F) Purified phagosomes at 1 and 5 h post internalization of OVA-coated 3-μm magnetic beads from WT and *GRASP55*^{-/-} BMDCs were incubated with (E) CD8⁺ B3Z and (F) CD4⁺ OT-IIL T cells to evaluate antigen-specific activation. Dashed lines show the background signal obtained by incubating an excess of non-internalized OVA-coated beads with T cells.

Data represent mean ± SEM of triplicate values from 2 independent experiments. Unpaired two-tailed Student's t test was performed. See also Figure S5.

differences in MHC-I and MHC-II presentation between WT and *GRASP55*^{-/-} BMDCs (Figures 7A and 7B). In contrast, the presentation of *E. coli*-expressing OVA by both MHC-I and -II was significantly reduced in *GRASP55*^{-/-} BMDCs, as compared to WT cells (Figures 7C and 7D, respectively).

To address the mechanisms underlying this discrepancy in the dependency on GRASP55 for antigen presentation of these two microbes, we explored whether GRASP55 is efficiently recruited to the *T. gondii* PV and *E. coli*-containing phagosomes. We infected BMDCs with the green fluorescent strain TgRH



(legend on next page)

YFP/SAG1-OVA and labeled GRA2 (PVs containing actively invaded, live parasites), and GRASP55. GRASP55 localizes very close to the PV but does not co-localize with GRA2 or YFP (Figure 7E). To further elaborate this location of GRASP55, we performed super-resolution (single-molecule localization) microscopy and confirmed that GRASP55 is indeed excluded from the PV (Figure 7F). We used a similar approach to study the recruitment of GRASP55 to *E. coli* phagosomes. We incubated BMDCs with pH-sensitive green *E. coli* bioparticles, immunostained GRASP55, and visualized the cells by confocal microscopy. GRASP55 displayed clear co-localization with *E. coli*-containing phagosomes, distinct from its intracellular pool at the Golgi apparatus, suggesting its redistribution to intercept bacterial phagosomes (Figure 7G). These data reveal that GRASP55 expression is critical to achieve efficient presentation of *E. coli* antigens, but not of *T. gondii* antigens, to CD8⁺ and CD4⁺ T cells.

Altogether, the data obtained in our study highlight the main relevance of GRASP55 to control exogenous antigen presentation by promoting optimal transport of pMHC-I and -II molecules from BMDC phagosomes to the plasma membrane.

DISCUSSION

Our findings show that GRASP55 is recruited to late BMDC phagosomes. This suggests that GRASP55 plays a specific role in the final trafficking steps of pMHC to the plasma membrane. Indeed, we confirmed that GRASP55 is a key regulator of the transport of both MHC-I and -II molecules loaded with antigenic peptides. Notably, we observed a significant accumulation of MHC-I/OVA complexes in GRASP55^{-/-} 5-h phagosomes, as detected using the SIINFEKL-H-2K^b-specific monoclonal antibody 25.D1. Additionally, we developed an experimental approach involving the purification of 3-μm OVA-coated magnetic beads. Using this method, we found enhanced activation of CD8⁺ and CD4⁺ T cells after incubation with GRASP55^{-/-} 5-h phagosomes but not 1-h phagosomes. These results were striking, as, to date, no common molecular regulator of the export of both MHC-I and -II molecules from phagosomal membranes to the cell surface has been identified. This is especially true for antigen

cross-presentation, where such mechanisms remain largely unknown.

While the endosomal recycling pathway has been suggested to control the final transport of pMHC-I molecules from phagosomes, direct evidence to support this hypothesis is lacking.^{26,32,33} Regarding MHC-II antigen presentation, several molecular factors have been identified to regulate the transport of pMHC-II molecules to the cell surface, including Rab7, which may recruit dynein to regulate trafficking³⁴; the small GTPase ARL14, which controls myosin 1E and MHC-II transport³⁵; and adaptor protein 3, which regulates the phagosomal delivery of pMHC-II molecules in a TLR4-dependent manner.³⁶ In contrast, here we demonstrate that GRASP55 plays a central role in the transport of both MHC-I and -II molecules loaded with antigenic peptides.

Knockout of GRASPs in cells and mice has no obvious effects on the structure of the Golgi stack.^{37,38} We further demonstrated that the single GRASP gene *GRH1*, in slime molds and yeast, is required for the unconventional secretion of AcbA and Acb1, respectively.^{39,40} Our new findings reveal that GRASP55 plays a role in the presentation of exogenous antigens bound to MHC-I and -II molecules, but its significance becomes apparent only under inflammatory conditions (in BMDCs). Specifically, we observed that cells lacking GRASP55 arrest pMHC molecules in BMDC phagosomes, a compartment that shares many similarities with CUPS in yeast.

In a previous study, we also demonstrated that GRASP55 controls the secretion of IL-1β from macrophages stimulated with LPS and ATP.¹⁶ Moreover, it has been reported that inhibition of mTORC1 relocates GRASP55 to a compartment associated with unconventional protein secretion.⁴¹ This further supports GRASP55's role in stress-induced secretion of various cargos in a cell-type-specific manner. The exact function of GRASP55 in unconventional secretion remains unclear, but one possibility is that GRASPs are required for the extraction of pMHC complexes from phagosomes into small vesicles that traffic to the cell surface.

In summary, we conclude that BMDC phagosomes receive two important inputs from the secretory pathway during exogenous antigen presentation. First, an early recruitment of ERGIC-derived vesicles in a Sec22b-dependent manner

Figure 6. GRASP55 is not required for antigen internalization or phagosomal maturation in BMDCs

- (A–D) Evaluation of endocytosis and phagocytosis by WT and GRASP55^{-/-} BMDCs. Shown is fluid-phase endocytosis of fluorescent OVA (conjugated to Alexa 647) and phagocytosis of fluorescent OVA-coated 3-μm latex beads after 1 h of internalization.
- (A) Representative FACS profiles of OVA-A647 fluorescence intensity at the indicated concentrations and temperatures.
- (B) Histogram showing the MFI quantification of Alexa 647 in WT and GRASP55^{-/-} BMDCs.
- (C) Representative FACS profiles of WT and GRASP55^{-/-} BMDCs after phagocytosis. Red numbers indicate the percentage of cells that have completely internalized particles (A647⁺/A488⁻).
- (D) Histogram showing the percentage of efficient phagocytosis by WT and GRASP55^{-/-} BMDCs.
- (B and D) Data represent mean ± SEM of triplicate values from 3 independent experiments. Unpaired two-tailed Student's t test was performed.
- (E–H) WT and GRASP55^{-/-} BMDCs were incubated with OVA-coated 3-μm latex beads for 15, 60, and 180 min.
- (E) Representative FACS profiles showing OVA staining on isolated phagosomes.
- (F) Histogram showing the kinetics of OVA degradation as a percentage of intact OVA in isolated phagosomes.
- (G) Representative FACS profiles showing Lamp1 staining on isolated phagosomes. Red numbers indicate the percentage of Lamp1⁺ phagosomes.
- (H) Histogram showing the kinetics of Lamp1 acquisition (percentage fluorescein isothiocyanate⁺) in isolated phagosomes.
- (F and H) Data represent mean ± SEM of triplicate values from 3 independent experiments. $p > 0.05$ (ns). A two-way ANOVA and Bonferroni post-test were performed.

See also Figure S6.

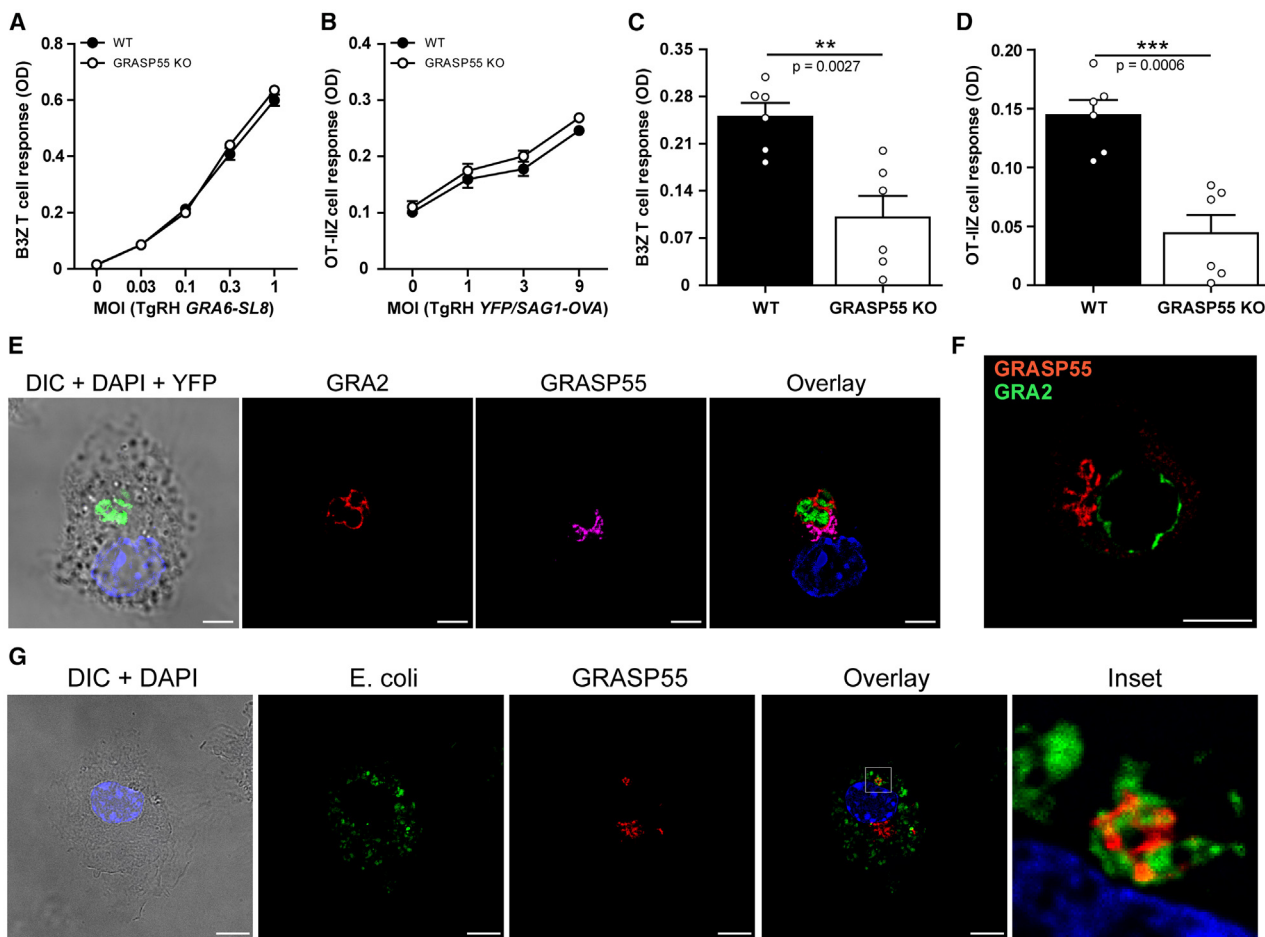


Figure 7. *T. gondii* and *E. coli* antigen presentation by WT and GRASP55^{-/-} BMDCs

(A and B) MHC-I presentation of the *T. gondii* GRA6 antigen from the parasite strain TgRH GRA6-SL8 (A) and MHC-II presentation of OVA associated with the *T. gondii* strain TgRH YFP SAG1-OVA (B) after 12 h of infection were evaluated. Data show mean ± SEM of triplicate values and are representative of 4 independent experiments. $p > 0.05$ (ns). A two-way ANOVA and Bonferroni post-test were performed.

(C and D) MHC-I cross-presentation (C) and MHC-II presentation (D) of *E. coli* DH5 α -expressing OVA after 12 h of infection were evaluated. Data represent mean ± SEM of triplicate values from 2 independent experiments. Unpaired two-tailed Student's t test was performed.

(E) WT BMDCs were infected with the *T. gondii* strain TgRH YFP SAG1-OVA for 12 h, and confocal images detecting GRA2 (red) and GRASP55 (magenta) were taken. DAPI (blue), the fluorescent parasite (green), and DIC are shown on the left. The overlay of all fluorescent channels is shown on the right. Scale bars: 5 μ m. Data are representative of at least 30 images analyzed from 3 independent experiments. Pearson correlation coefficient = 0.08405.

(F) Immunofluorescence labeling and stimulated emission depletion (STED) microscopy analysis showing the PV in green by detection of GRA2 and the host protein GRASP55 (red) in a WT BMDC infected with TgRH GRA6-SL8 for 12 h. Scale bars: 5 μ m. Data are representative of 10 images analyzed from 2 independent experiments. Pearson correlation coefficient = 0.01129.

(G) WT BMDCs were incubated with pH-sensitive *E. coli* particles (green) for 12 h, and confocal images were taken to detect GRASP55 (red). DAPI (blue) and DIC are shown on the left. The overlay of all fluorescent channels is shown on the right. The white box is shown at higher magnification in the inset. Scale bars: 5 μ m. Data are representative of at least 30 images analyzed from 3 independent experiments.

enables BMDC phagosomes to acquire the PLC and other relevant molecules necessary for efficient cross-presentation.³ Second, there is a later interaction with *cis* Golgi-derived vesicles, which delivers GRASP55 to phagosomal membranes, facilitating the subsequent export of pMHC molecules to the cell surface. These two interactions between BMDC phagosomes and the early secretory pathway are likely independent of the phagosomal connections with the endosomal recycling compartment and MIIC for the recruitment of MHC-I and -II molecules, respectively.

Limitations of the study

We note three main limitations: (1) discrepancy regarding the relevance of GRASP55 for exogenous antigen presentation between GRASP55^{-/-} BMDCs and splenic DCs, (2) the lack of Graspin specificity in the MHC-II antigen presentation pathway, and (3) the absence of a clear molecular mechanism underlying GRASP55 function in BMDCs.

Regarding the first point, we did not observe a defective phenotype for antigen presentation in GRASP55^{-/-} tissue-resident DCs as seen in BMDCs. This can be partially explained by

the relatively mild expression of GRASP55 in total splenic DCs. However, we did not evaluate potential differential expression of GRASP55 in splenic DC subsets. Although the antigen presentation data from splenic DCs were somewhat disappointing, they highlight the important and specific role of GRASP55 in inflammatory DCs, suggesting new avenues for exploring alternative mechanisms in different DC subsets.

The second limitation concerns the use of Graspin in the MHC-II presentation pathway. Treatment of *GRASP55*^{-/-} BMDCs with Graspin further inhibited CD4⁺ T cell activation. These results demonstrate the proper specificity of Graspin in targeting GRASP55 in the context of MHC-I cross-presentation but also reveal a non-specific effect of this inhibitor on MHC-II antigen presentation.

The third limitation relates to the unknown specific function of GRASP55. As a result, its precise role in BMDC phagosomes remains unclear. Based on previous studies from our group and others related to the unconventional secretion of proteins, we can speculate that GRASP55 is required to organize or extract membrane domains containing pMHC complexes from phagosomes into small vesicles that traffic to the cell surface. Ongoing and future studies in these areas will help clarify the critical roles of GRASP proteins in the presentation of exogenous antigens.

RESOURCE AVAILABILITY

Lead contact

Requests for further information, resources, and reagents should be directed to and will be fulfilled by the lead contact, Vivek Malhotra (vivek.malhotra@crg.eu).

Materials availability

This study did not generate unique reagents.

Data and code availability

- All data reported in this paper will be shared by the [lead contact](#) upon request.
- This paper does not report original code.
- Any additional information required to re-analyze the data reported in this paper is available from the [lead contact](#) upon request.

ACKNOWLEDGMENTS

We thank all members of the Malhotra and Blanchard laboratories, especially Emilie Bassot for technical assistance. We thank the joint CRG/UPF FACS Unit at Parc de Recerca Biomèdica de Barcelona (PRBB), the Advanced Light Microscopy Unit at the CRG, and the Cell Imaging facility of the Infinity Institute, especially Sophie Allart, for valuable help. We acknowledge support from the Spanish Ministry of Science and Innovation to the EMBL partnership, the Centro de Excelencia Severo Ochoa, and the CERCA Programme/Generalitat de Catalunya. V.M. is an Institució Catalana de Recerca i Estudis Avançats professor at the CRG. Work in the V.M. laboratory is funded by grants from the Spanish Ministry of Economy and Competitiveness (Plan Nacional to V.M., PID2019-105518GB-I00) and the European Research Council Synergy Grant (ERC-2020-SyG - Proposal 951146). I.C. was funded by the Consejo Nacional de Investigaciones Científicas y Técnicas (CONICET), Argentina, and by project PCI2021-122039-2B, funded by MCIN/AEI/10.13039/501100011033 and the European Union NextGenerationEU/PRTR. N. Blanchard was supported by grants from the PIA PARAFRAP Consortium (ANR-11-LABX0024) and Agence Nationale de la Recherche (ANR-19-CE15-0008 TRANSMIT and ANR-22-CE14-0053 NINTENDO). D.S. was funded by MCIN PID2022-137712OB-I00 MCIN/AEI/10.13039/501100011033 Agencia Estatal de Inves-

tigación, European Union NextGenerationEU/PRTR. This work reflects only the authors' views, and the EU Community is not liable for any use that may be made of the information contained therein.

AUTHOR CONTRIBUTIONS

I.C. and V.M. conceived and supervised the project. I.C., R.T., N. Blanchard, D.S., and V.M. designed experiments and provided critical reagents. I.C., M.J.P.R., and N. Brouwer handled mice for experiments and provided technical assistance. I.C., S.D., M.J.P.R., E.P., M.B., and J.B. performed experiments. I.C. and V.M. wrote the manuscript. S.D., E.P., J.B., R.T., N. Blanchard, and D.S. contributed to manuscript editing. All authors discussed results and data analysis and commented on manuscript preparation.

DECLARATION OF INTERESTS

The authors declare no competing interests.

STAR METHODS

Detailed methods are provided in the online version of this paper and include the following:

- [KEY RESOURCES TABLE](#)
- [EXPERIMENTAL MODEL AND STUDY PARTICIPANT DETAILS](#)
 - Mice and cells
- [METHOD DETAILS](#)
 - *In silico* analyses
 - Immunoblotting
 - qPCR
 - Flow cytometry
 - Phagosome purification
 - Exogenous antigen presentation
 - Endogenous MHC-I antigen presentation
 - Immunofluorescence and microscopy
- [QUANTIFICATION AND STATISTICAL ANALYSIS](#)
 - Statistical analysis

SUPPLEMENTAL INFORMATION

Supplemental information can be found online at <https://doi.org/10.1016/j.celrep.2025.115333>.

Received: March 13, 2024

Revised: October 14, 2024

Accepted: January 28, 2025

Published: February 15, 2025

REFERENCES

1. Kotsias, F., Cebrían, I., and Alloatti, A. (2019). Antigen processing and presentation. *Int. Rev. Cell Mol. Biol.* 348, 69–121. <https://doi.org/10.1016/bs.ircmb.2019.07.005>.
2. Blum, J.S., Wearsch, P.A., and Cresswell, P. (2013). Pathways of antigen processing. *Annu. Rev. Immunol.* 31, 443–473. <https://doi.org/10.1146/annurev-immunol-032712-095910>.
3. Cebrían, I., Visentini, G., Blanchard, N., Jouve, M., Bobard, A., Moita, C., Enninga, J., Moita, L.F., Amigorena, S., and Savina, A. (2011). Sec22b regulates phagosomal maturation and antigen crosspresentation by dendritic cells. *Cell* 147, 1355–1368. <https://doi.org/10.1016/j.cell.2011.11.021>.
4. Blander, J.M. (2023). Different routes of MHC-I delivery to phagosomes and their consequences to CD8 T cell immunity. *Semin. Immunol.* 66, 101713. <https://doi.org/10.1016/j.smim.2023.101713>.
5. Warmerdam, P.A., Long, E.O., and Roche, P.A. (1996). Isoforms of the invariant chain regulate transport of MHC class II molecules to antigen

- processing compartments. *J. Cell Biol.* 133, 281–291. <https://doi.org/10.1083/jcb.133.2.281>.
6. Roche, P.A., Teletski, C.L., Stang, E., Bakke, O., and Long, E.O. (1993). Cell surface HLA-DR-invariant chain complexes are targeted to endosomes by rapid internalization. *Proc. Natl. Acad. Sci. USA* 90, 8581–8585. <https://doi.org/10.1073/pnas.90.18.8581>.
 7. McCormick, P.J., Martina, J.A., and Bonifacino, J.S. (2005). Involvement of clathrin and AP-2 in the trafficking of MHC class II molecules to antigen-processing compartments. *Proc. Natl. Acad. Sci. USA* 102, 7910–7915. <https://doi.org/10.1073/pnas.0502206102>.
 8. Mantegazza, A.R., Magalhaes, J.G., Amigorena, S., and Marks, M.S. (2013). Presentation of phagocytosed antigens by MHC class I and II. *Traffic* 14, 135–152. <https://doi.org/10.1111/tra.12026>.
 9. Yang, J., Rong, S.-J., Zhou, H.-F., Yang, C., Sun, F., and Li, J.-Y. (2023). Lysosomal control of dendritic cell function. *J. Leukoc. Biol.* 114, 518–531. <https://doi.org/10.1093/jleuko/qjad117>.
 10. Bruns, C., McCaffery, J.M., Curwin, A.J., Duran, J.M., and Malhotra, V. (2011). Biogenesis of a novel compartment for autophagosome-mediated unconventional protein secretion. *J. Cell Biol.* 195, 979–992. <https://doi.org/10.1083/jcb.201106098>.
 11. Cruz-Garcia, D., Malhotra, V., and Curwin, A.J. (2018). Unconventional protein secretion triggered by nutrient starvation. *Semin. Cell Dev. Biol.* 83, 22–28. <https://doi.org/10.1016/j.semcd.2018.02.021>.
 12. Fontana, N.A., Fonseca-Maldonado, R., Mendes, L.F.S., Meleiro, L.P., and Costa-Filho, A.J. (2018). The yeast GRASP Grh1 displays a high polypeptide backbone mobility along with an amyloidogenic behavior. *Sci. Rep.* 8, 15690. <https://doi.org/10.1038/s41598-018-33955-1>.
 13. Behnia, R., Barr, F.A., Flanagan, J.J., Barlowe, C., and Munro, S. (2007). The yeast orthologue of GRASP65 forms a complex with a coiled-coil protein that contributes to ER to Golgi traffic. *J. Cell Biol.* 176, 255–261. <https://doi.org/10.1083/jcb.200607151>.
 14. Immudb <http://immudb.bjmu.edu.cn/immuco.html>.
 15. Gene Skyline <http://rstats.immgen.org/Skyline/skyline.html>.
 16. Chirtoiu, M., Brouwers, N., Turacchio, G., Pirozzi, M., and Malhotra, V. (2019). GRASP55 and UPR control interleukin-1 β aggregation and secretion. *Dev. Cell* 49, 145–155.e4. <https://doi.org/10.1016/j.devcel.2019.02.011>.
 17. Kimura, T., Jia, J., Kumar, S., Choi, S.W., Gu, Y., Mudd, M., Dupont, N., Jiang, S., Peters, R., Farzam, F., et al. (2017). Dedicated SNAREs and specialized TRIM cargo receptors mediate secretory autophagy. *EMBO J.* 36, 42–60. <https://doi.org/10.15252/embj.201695081>.
 18. Cartier-Michaud, A., Bailly, A.-L., Betzi, S., Shi, X., Lissitzky, J.-C., Zarubica, A., Sergé, A., Roche, P., Lugari, A., Hamon, V., et al. (2017). Genetic, structural, and chemical insights into the dual function of GRASP55 in germ cell Golgi remodeling and JAM-C polarized localization during spermatogenesis. *PLoS Genet.* 13, e1006803. <https://doi.org/10.1371/journal.pgen.1006803>.
 19. Wang, P., Qi, H., Song, S., Li, S., Huang, N., Han, W., and Ma, D. (2015). ImmuCo: a database of gene co-expression in immune cells. *Nucleic Acids Res.* 43, D1133–D1139. <https://doi.org/10.1093/nar/gku980>.
 20. Jiang, X., Shen, C., Rey-Ladino, J., Yu, H., and Brunham, R.C. (2008). Characterization of murine dendritic cell line JAWS II and primary bone marrow-derived dendritic cells in Chlamydia muridarum antigen presentation and induction of protective immunity. *Infect. Immun.* 76, 2392–2401. <https://doi.org/10.1128/IAI.01584-07>.
 21. Croce, C., Garrido, F., Dinamarca, S., Santi-Rocca, J., Marion, S., Blanchard, N., Mayorga, L.S., and Cebrían, I. (2022). Efficient cholesterol transport in dendritic cells defines optimal exogenous antigen presentation and *Toxoplasma gondii* proliferation. *Front. Cell Dev. Biol.* 10, 837574. <https://doi.org/10.3389/fcell.2022.837574>.
 22. Alloatti, A., Kotsias, F., Magalhaes, J.G., and Amigorena, S. (2016). Dendritic cell maturation and cross-presentation: timing matters. *Immunol. Rev.* 272, 97–108. <https://doi.org/10.1111/imr.12432>.
 23. Stein, M.F., Blume, K., Heilingloh, C.S., Kummer, M., Biesinger, B., Sticht, H., and Steinkasserer, A. (2015). CD83 and GRASP55 interact in human dendritic cells. *Biochem. Biophys. Res. Commun.* 459, 42–48. <https://doi.org/10.1016/j.bbrc.2015.02.057>.
 24. Iborra, S., Izquierdo, H.M., Martínez-López, M., Blanco-Menéndez, N., Reis e Sousa, C., and Sancho, D. (2012). The DC receptor DNGR-1 mediates cross-priming of CTLs during vaccinia virus infection in mice. *J. Clin. Investig.* 122, 1628–1643. <https://doi.org/10.1172/JCI60660>.
 25. Feinstein, T.N., and Linstedt, A.D. (2008). GRASP55 regulates Golgi ribbon formation. *Mol. Biol. Cell* 19, 2696–2707. <https://doi.org/10.1091/mbc.E07-11-1200>.
 26. Cebrían, I., Croce, C., Guerrero, N.A., Blanchard, N., and Mayorga, L.S. (2016). Rab22a controls MHC-I intracellular trafficking and antigen cross-presentation by dendritic cells. *EMBO Rep.* 17, 1753–1765. <https://doi.org/10.1525/embr.201642358>.
 27. Lin, M.L., Zhan, Y., Proietto, A.I., Prato, S., Wu, L., Heath, W.R., Villadangos, J.A., and Lew, A.M. (2008). Selective suicide of cross-presenting CD8+ dendritic cells by cytochrome c injection shows functional heterogeneity within this subset. *Proc. Natl. Acad. Sci. USA* 105, 3029–3034. <https://doi.org/10.1073/pnas.0712394105>.
 28. Croce, C., Mayorga, L.S., and Cebrían, I. (2020). Differential requirement of Rab22a for the recruitment of ER-derived proteins to phagosomes and endosomes in dendritic cells. *Small GTPases* 11, 211–219. <https://doi.org/10.1080/21541248.2017.1384088>.
 29. Poncet, A.F., Blanchard, N., and Marion, S. (2019). Toxoplasma and dendritic cells: an intimate relationship that deserves further scrutiny. *Trends Parasitol.* 35, 870–886. <https://doi.org/10.1016/j.pt.2019.08.001>.
 30. Blanchard, N., Gonzalez, F., Schaeffer, M., Joncker, N.T., Cheng, T., Shastri, A.J., Robey, E.A., and Shastri, N. (2008). Immunodominant, protective response to the parasite *Toxoplasma gondii* requires antigen processing in the endoplasmic reticulum. *Nat. Immunol.* 9, 937–944. <https://doi.org/10.1038/ni.1629>.
 31. Lopez, J., Bittame, A., Massera, C., Vasseur, V., Effantin, G., Valat, A., Buaillon, C., Allart, S., Fox, B.A., Rommereim, L.M., et al. (2015). Intravacuolar membranes regulate CD8 T cell recognition of membrane-bound *Toxoplasma gondii* protective antigen. *Cell Rep.* 13, 2273–2286. <https://doi.org/10.1016/j.celrep.2015.11.001>.
 32. Nair-Gupta, P., Baccarini, A., Tung, N., Seyffer, F., Florey, O., Huang, Y., Banerjee, M., Overholtzer, M., Roche, P.A., Tampé, R., et al. (2014). TLR signals induce phagosomal MHC-I delivery from the endosomal recycling compartment to allow cross-presentation. *Cell* 158, 506–521. <https://doi.org/10.1016/j.cell.2014.04.054>.
 33. Montealegre, S., and van Endert, P.M. (2018). Endocytic recycling of MHC class I molecules in non-professional antigen presenting and dendritic cells. *Front. Immunol.* 9, 3098. <https://doi.org/10.3389/fimmu.2018.03098>.
 34. Jordens, I., Fernandez-Borja, M., Marsman, M., Dusseljee, S., Janssen, L., Calafat, J., Janssen, H., Wubbolts, R., and Neefjes, J. (2001). The Rab7 effector protein RILP controls lysosomal transport by inducing the recruitment of dynein-dynactin motors. *Curr. Biol.* 11, 1680–1685. [https://doi.org/10.1016/S0960-9822\(01\)00531-0](https://doi.org/10.1016/S0960-9822(01)00531-0).
 35. Paul, P., van den Hoorn, T., Jongsma, M.L.M., Bakker, M.J., Hengeveld, R., Janssen, L., Cresswell, P., Egan, D.A., van Ham, M., Ten Brinke, A., et al. (2011). A Genome-wide multidimensional RNAi screen reveals pathways controlling MHC class II antigen presentation. *Cell* 145, 268–283. <https://doi.org/10.1016/j.cell.2011.03.023>.
 36. Mantegazza, A.R., Guttentag, S.H., El-Benna, J., Sasai, M., Iwasaki, A., Shen, H., Laufer, T.M., and Marks, M.S. (2012). Adaptor Protein-3 in dendritic cells facilitates phagosomal Toll-like Receptor signaling and antigen presentation to CD4+ T cells. *Immunity* 36, 782–794. <https://doi.org/10.1016/j.jimmuni.2012.02.018>.
 37. Duran, J.M., Kinseth, M., Bossard, C., Rose, D.W., Polishchuk, R., Wu, C.C., Yates, J., Zimmerman, T., and Malhotra, V. (2008). The role of GRASP55 in Golgi fragmentation and entry of cells into mitosis. *Mol. Biol. Cell* 19, 2579–2587. <https://doi.org/10.1091/mbc.e07-10-0998>.

38. Grond, R., Veenendaal, T., Duran, J.M., Raote, I., van Es, J.H., Corstjens, S., Delfgou, L., El Haddouti, B., Malhotra, V., and Rabouille, C. (2020). The function of GORASPs in Golgi apparatus organization *in vivo*. *J. Cell Biol.* **219**, e202004191. <https://doi.org/10.1083/jcb.202004191>.
39. Kinseth, M.A., Anjard, C., Fuller, D., Guizzanti, G., Loomis, W.F., and Malhotra, V. (2007). The Golgi-associated protein GRASP is required for unconventional protein secretion during development. *Cell* **130**, 524–534. <https://doi.org/10.1016/j.cell.2007.06.029>.
40. Duran, J.M., Anjard, C., Stefan, C., Loomis, W.F., and Malhotra, V. (2010). Unconventional secretion of Acb1 is mediated by autophagosomes. *J. Cell Biol.* **188**, 527–536. <https://doi.org/10.1083/jcb.200911154>.
41. Nüchel, J., Tauber, M., Nolte, J.L., Mörgelin, M., Türk, C., Eckes, B., Demetriadis, C., and Plomann, M. (2021). An mTORC1-GRASP55 signaling axis controls unconventional secretion to reshape the extracellular proteome upon stress. *Mol. Cell* **81**, 3275–3293.e12. <https://doi.org/10.1016/j.molcel.2021.06.017>.
42. Murray, A., Mercier, C., Decoster, A., Lecordier, L., Capron, A., and Cesbron-Delaunay, M.F. (1993). Multiple B-cell epitopes in a recombinant GRA2 secreted antigen of *Toxoplasma gondii*. *Appl. Parasitol.* **34**, 235–244.
43. van Ziel, A.M., Largo-Barrientos, P., Wolzak, K., Verhage, M., and Schepers, W. (2019). Unconventional secretion factor GRASP55 is increased by pharmacological unfolded protein response inducers in neurons. *Sci. Rep.* **9**, 1567. <https://doi.org/10.1038/s41598-018-38146-6>.

STAR★METHODS

KEY RESOURCES TABLE

REAGENT or RESOURCE	SOURCE	IDENTIFIER
Antibodies		
Rabbit polyclonal anti-GRASP55	Invitrogen (Thermo)	Cat# PA5-57210; RRID: AB_2642205
Mouse monoclonal anti-SIINFEKL7H-2K ^b (clone 25-D1.16) conjugated to APC	Invitrogen (Thermo)	Cat# 17-5743-80; RRID: AB_1311288
Rat monoclonal anti-CD83 (clone Michel-17) conjugated to FITC	Invitrogen (Thermo)	Cat# 11-0831-82; RRID: AB_465141
Rat monoclonal anti-mouse IFN-γ (clone XMG1.2) conjugated to APC	Invitrogen (Thermo)	Cat# 17-7311-82; RRID: AB_469504
Goat polyclonal anti-GRASP65	Santa Cruz	Cat# sc-19481; RRID: AB_2232631
Mouse monoclonal anti-β-actin	Sigma-Aldrich	Cat# A1978; RRID: AB_476692
Rabbit polyclonal anti-chicken egg albumin antibody (whole antiserum)	Sigma-Aldrich	Cat# C6534; RRID: AB_258953
Rabbit polyclonal anti-ERGIC-53/p58	Sigma-Aldrich	Cat# E6782; RRID: AB_1840849
Goat anti-rabbit STAR RED	Sigma-Aldrich	Cat# 41699; RRID: AB_2928168
Goat anti-mouse STAR 580	Sigma-Aldrich	Cat# 52403; RRID: AB_2923543
Mouse monoclonal anti-PDI	Enzo Life Science	Cat# ALX-804-012-R100; RRID: AB_2052192
Mouse monoclonal anti-TGN46	Abcam	Cat# ab2809; RRID: AB_2203290
Mouse monoclonal anti-GM130	BD Transduction Laboratories	Cat# 610822; RRID: AB_398141
Mouse monoclonal anti-rat TGN38	BD Transduction Laboratories	Cat# 610898; RRID: AB_398215
Rat anti-Lamp1	BD Pharmingen	Cat# 553792; RRID: AB_2134499
Rat anti-Lamp1 conjugated to FITC	BD Pharmingen	Cat# 561069; RRID: AB_395057
Hamster anti-CD11c conjugated to PE-Cy7	BD Pharmingen	Cat# 561022; RRID: AB_2033997
Mouse anti-H-2K ^b conjugated to FITC	BD Pharmingen	Cat# 562002; RRID: AB_394927
Mouse anti-I-A ^b conjugated to PE	BD Pharmingen	Cat# 553552; RRID: AB_394919
Rat anti-CD86 conjugated to APC	BD Pharmingen	Cat# 561964; RRID: AB_2075114
Mouse monoclonal anti-GRA2 (Tg17-179)	Marie-France Cesbron-Delauw (Institute for Advanced Biosciences, Grenoble) Murray et al., 1993 ⁴²	N/A
Donkey anti-mouse Alexa Fluor 488	Invitrogen (Thermo)	Cat# A-21202; RRID: AB_141607
Donkey anti-mouse Alexa Fluor 555	Invitrogen (Thermo)	Cat# A-31570; RRID: AB_2536180
Donkey anti-mouse Alexa Fluor 647	Invitrogen (Thermo)	Cat# A-31571; RRID: AB_162542
Donkey anti-rabbit Alexa Fluor 555	Invitrogen (Thermo)	Cat# A-31572; RRID: AB_162543
Donkey anti-rabbit Alexa Fluor 647	Invitrogen (Thermo)	Cat# A-31573; RRID: AB_2536183
Donkey anti-mouse IgG-HRP	Jackson Laboratories	Cat# 715-035-151; RRID: AB_2340771
Donkey anti-rabbit IgG-HRP	Jackson Laboratories	Cat# 711-035-152; RRID: AB_10015282
Donkey anti-goat IgG-HRP	Jackson Laboratories	Cat# 705-035-147; RRID: AB_2313587
Donkey anti-rat IgG-HRP	Jackson Laboratories	Cat# 712-035-153; RRID: AB_2340639
Bacterial and virus strains		
<i>E. coli</i> DH5α expressing OVA	Nicolas Blanchard (Institute Infinity)	N/A
Vaccinia virus expressing OVA (VACV-OVA)	Jonathan W. Yewdell and Jack R. Bennink (National Institutes of Health, Bethesda, MD)	N/A
Chemicals, peptides, and recombinant proteins		
OVA peptide 257–264, SIINFEKL	Polypeptide Group	N/A
OVA peptide 323–339, ISQAVHAAHAEINEAGR	GenScript	Cat# RP10610

(Continued on next page)

Continued

REAGENT or RESOURCE	SOURCE	IDENTIFIER
OVA peptide 262–276, EKLTEWTSSNVMEER	GenScript	N/A
B8R peptide 20–27, TSYKFESV	GenScript	Cat# RP21086
GRASP55 inhibitor, Graspin	Vitas-M Chemical Laboratory, Limited	ID# STK700118
Critical commercial assays		
Ovalbumin, lyophilized powder	Worthington Biochemical Corporation	Cat# LS003056
Ovalbumin, Low Endo™, purified	Worthington Biochemical Corporation	Cat# LS003061
Lipopolysaccharide (LPS) from <i>E. coli</i> 0111:B4	Sigma-Aldrich	Cat# L4391
Brefeldin A (BFA)	Sigma-Aldrich	Cat# B7651
Ultrapure LPS from <i>E. coli</i> 0111:B4	InvivoGen	Cat# trl-3pelps
Class B CpG ODN 1668 - Murine TLR9 ligand	InvivoGen	Cat# trl-1668
FITC annexin V	BD Pharmingen	Cat# 556419; RRID: AB_2665412
Phalloidin conjugated to Alexa 488	Molecular Probes, Life Technologies (Thermo)	Cat# A12379
3-μm latex beads (polystyrene microspheres)	Polysciences Inc	Cat# 17134-15
3-μm Dynabeads M-270 Epoxy	Invitrogen (Thermo)	Cat# 14301
OVA conjugated to Alexa 647	Invitrogen (Thermo)	Cat# O34784
Mouse GM-CSF recombinant protein	Invitrogen (Thermo)	Cat# BMS325
Calcein AM	Invitrogen (Thermo)	Cat# C1430
pHrodo™ Green <i>E. Coli</i> BioParticles™	Invitrogen (Thermo)	Cat# P35366
Protease inhibitor cocktail	Roche	Cat# 04693132001
Chlorophenol red-β-D-galactopyranoside (CPRG)	Roche	Cat# 10884308001
CD11c MicroBeads UltraPure, mouse	Miltenyi Biotec	Cat# 130-125-835
Mouse Direct PCR kit	Biotools	Cat# B45012
RNeasy® Micro Kit	QIAGEN	Cat# 74004
SuperScript™ III First-Strand Synthesis System for RT-PCR	Invitrogen	Cat# 18080051
HOT FIREPol® EvaGreen® qPCR Supermix 5x	Solis BioDyne	Cat# 08-36-00001
MHC-I H2-K ^b /B8R _{20–27} tetramer	NIH Tetramer Facility at Emory University	N/A
Experimental models: Cell lines		
Bone-marrow-derived dendritic cells (BMDCs) WT	This paper	N/A
Bone-marrow-derived dendritic cells (BMDCs) GRASP55 ^{-/-}	This paper	N/A
B3Z CD8 ⁺ T cells	Nicolas Blanchard (Institute Infinity)	N/A
OT-II Z CD4 ⁺ T cells	Nicolas Blanchard (Institute Infinity)	N/A
JAWS-II DCs	Nicolas Blanchard (Institute Infinity)	ATCC CRL-3612
Human Foreskin Fibroblasts (HFFs)	Nicolas Blanchard (Institute Infinity)	ATCC SCRC-1041
RAW 264.7 macrophages	David Sancho (CNIC)	ATCC TIB-71
Experimental models: Organisms/strains		
Mouse: C57BL/6J WT	Chiritoiu et al., 2019 ¹⁶	N/A
Mouse: C57BL/6J GRASP55 ^{-/-}	Chiritoiu et al., 2019 ¹⁶	N/A
Mouse: B6/SJL 45.1+/C57BL/6J 45.2+ WT chimera	This paper	N/A
Mouse: B6/SJL 45.1+/C57BL/6J 45.2+ GRASP55 ^{-/-} chimera	This paper	N/A
<i>Toxoplasma gondii</i> : TgRH GRA6-OVA	Nicolas Blanchard (Institute Infinity) ²¹	N/A
<i>Toxoplasma gondii</i> : TgRH YFP SAG1-OVA	Nicolas Blanchard (Institute Infinity) ³	N/A

(Continued on next page)

Continued

REAGENT or RESOURCE	SOURCE	IDENTIFIER
Oligonucleotides		
Genotyping primer F: 5'-cgatcccccctcagccgtcagc-3'	Chiritoiu et al., 2019 ¹⁶	N/A
Genotyping primer R-1: 5'-cctcaaggccctaccttagc-3'	Chiritoiu et al., 2019 ¹⁶	N/A
Genotyping primer R-2: 5'-tgaactgtggcagctcagacc-3'	Chiritoiu et al., 2019 ¹⁶	N/A
GRASP55 qPCR primer F: 5'-catgtgctggaaagtggaaatc-3'	van Ziel et al., 2019 ⁴³	N/A
GRASP55 qPCR primer R: 5'-gctgaacaggcttcagactca-3'	van Ziel et al., 2019 ⁴³	N/A
GAPDH qPCR primer F: 5'-gcacagtcaacggccgagaat-3'	Invitrogen	N/A
GAPDH qPCR primer R: 5'-gccttctccatggtgaaat-3'	Invitrogen	N/A
Software and algorithms		
GraphPad Prism 5	GraphPad	N/A
FlowJo v10.10	FlowJo LLC	N/A
Fiji-ImageJ	NIH	N/A
Quantity One 4.6.6 software	Bio-Rad	N/A
ImmCo database	Wang et al., 2015 ¹⁹	N/A
Gene Skyline	Immunological Genome Project	N/A

EXPERIMENTAL MODEL AND STUDY PARTICIPANT DETAILS

Mice and cells

The GRASP55 (GORASP2) knockout mice were generated at McLaughlin Research Institute (Great Falls, Montana, US) using the EUCOMM/KOMP knockout first conditional-ready targeted ES cell resource (<http://www.mousephenotype.org/about-ikmc/eucomm-proram/eucomm-targeting-strategies>; targeted trap tm1a allele), as described in a previous study.¹⁶ C57BL/6 wild-type conditional knockout (cKO) and null mice used in our experiments were generated by crossing heterozygote cKO/null mice. The following primers were used to genotype the offspring with genomic DNA extracted from ear punches (Mouse Direct PCR kit, Biologics): 5'-ccgatcccccctcagccgtcagc-3', 5'-cctcaaggccctaccttagc-3' and 5'-tgaactgtggcagctcagacc-3'. All animals were maintained under specific pathogen-free conditions at 22°C and given access to food and water *ad libitum*. Mice with age between 12 and 16 weeks of both sexes were used for all experiments. To obtain bone marrow stem cells from femur and tibia, and DCs from spleen, animals were sacrificed in the Animal Facility of the Barcelona Biomedical Research Park (PRBB, Barcelona) by using a procedure approved by the local ethics committee 'Comité Ético de Experimentación Animal del PRBB' (CEEA-PRBB); procedure number NBO-22-0045. *In vivo* experiments were performed at the CNIC (Madrid) by using standard procedures approved by the local ethics committee 'Comité de Ética de Experimentación Animal' (CEEA-CNIC); procedure numbers PROEX 236/16, PROEX 301.5/21 and PROEX 302.6/21. All animal procedures complied with the EU Directive 2010/63/EU and the Commission Recommendation 2007/526/EC regarding the protection of animals used for experimental research, enforced in Spanish law under Real Decreto 53/2013.

Bone marrow cells were maintained in IMDM medium supplemented with 10% FBS and 20 ng/mL of recombinant mouse Granulocyte Macrophage Colony Stimulating Factor (rmGM-CSF) to induce BMDC differentiation. After 7 days, immature WT and GRASP55^{-/-} BMDCs were used for experimental work. JAWS-II DCs were maintained in culture by using 5 ng/mL rmGM-CSF-containing medium (IMDM) with 10% FBS. JAWS-II DCs were expanded and diluted every 2–4 days, depending on their growth rates. B3Z and OT-IIZ T cells were cultured with RPMI complete medium (10% FBS). *T. gondii* parasites were grown through continuous infection of Human Foreskin Fibroblasts (HFF), which were maintained in DMEM complete medium (10% FBS). Intracellular parasites were recovered after HFF disruption by the use of a 23-G needle. DH5 α *E. coli*-expressing OVA were grown in LB Broth medium with 100 μ g/mL ampicillin, and stimulated with 0.2 mM IPTG for 6 h before the antigen presentation experiments. Fetal Bovine Serum (FBS), IMDM, DMEM, and RPMI media were purchased in Gibco.

METHOD DETAILS

In silico analyses

To determine the co-expression profiles of GRASP55 and GRASP65 in mouse and human DCs, we used the ImmCo database (collected from microarray data)¹⁹ by choosing GRASP55 (Gorasp2) and GRASP65 (Gorasp1) as initial input in the Gene A and Gene B textboxes, respectively. As queries output, two separate downloadable CSV files containing the GEO sample names, the complete list of signal values corresponding to gene expression intensity, detection calls and *p* values were displayed. A total of 347 GRASP55 and GRASP65 signal values and 406 GRASP55 and GRASP65 signal values for mouse and human DCs were displayed, respectively. Finally, all mouse and human DCs signal values were plotted in a bar graph using the GraphPad Prism 5 software.

Immunoblotting

Purified phagosomes (10 µg) or total cell lysates from BMDCs, JAWS-II DCs and splenic DCs (10⁵ cells, around 50 µg of proteins for BMDCs and JAWS-II DCs, or around 25 µg of proteins for splenic DCs) were subjected to SDS-PAGE on 4–15% polyacrylamide gels. After transfer, the membranes were blocked in 5% Milk/TBS for 1 h and incubated ON with the following antibodies according to the experimental requirement: anti-GRASP65, anti-GRASP55, anti-β-actin, anti-OVA, and anti-Lamp1. Then, membranes were incubated for 1 h with secondary horseradish-peroxidase-conjugated antibodies. Bound antibodies were revealed using the Pierce ECL Western Blotting Substrate (ThermoFisher Scientific), according to the manufacturers' instructions. The intensity of the bands was quantified by densitometry using Quantity One 4.6.6 software (Bio-Rad) and was expressed as arbitrary units.

qPCR

Splenic DCs were treated with 50 µM of Graspin, 100 ng/mL of *E. coli*-derived ultrapure LPS (TLR4 ligand), or 5 µM of Class B CpG (TLR9 ligand) for 4 h at 37°C. Cell homogenization and RNA extraction were performed by using the RNeasy Micro Kit following the manufacturers' instructions. After determining RNA concentration, cDNA was produced with the SuperScript III First-Strand Synthesis System for RT-PCR, and PCR amplification was performed by using HOT FIREPol EvaGreen qPCR Supermix 5x during 40 cycles with the LightCycler 480 Instrument II (Roche). GAPDH/GRASP55 normalization was done by midpoint slope determination.

Flow cytometry

5 × 10⁵ BMDCs and JAWS-II DCs were incubated with 15, 30, or 60 µM of Graspin for 5 h. Cells were washed with 2% (w/v) PBS/BSA and labeled with 1 µg/mL of Calcein AM for 20 min at room temperature (at dark). After one wash with complete medium, cells were resuspended in 2% (w/v) BSA/PBS and just before FACS analysis DAPI at 3 µM (final concentration) was added.

For cell surface staining, WT and GRASP55^{−/−} BMDCs were collected, washed and incubated or not with 10 µg/mL LPS for 20 h. After washing with PBS, BMDCs were stained with a mix of FITC anti-H2K^b, PE anti-I-A^b, PE-Cy7 anti-CD11a and APC anti-CD86 for 45 min at 4°C. Cells were washed three times with 2% (w/v) BSA/PBS and analyzed by FACS.

For phagosomal isolation experiments, WT and GRASP55^{−/−} BMDCs were pulsed for 20 min at 18°C and 15 min at 37°C with 3-µm OVA-coated latex beads. Then, cells were washed once with cold 2% (w/v) BSA/PBS and twice with 1 mL of FBS, and chased for the indicated times with complete GM-CSF-containing medium at 37°C. After each chase period, BMDCs were washed once with cold 2% (w/v) BSA/PBS to stop phagocytosis, and then they were disrupted with a syringe (22G needle) in homogenization buffer (PBS 8% sucrose, 3 mM imidazole, 1 mM DTT, and 1X protease inhibitor cocktail), as we have described before.^{3,26} Samples were centrifuged at 150 g during 5 min at 4°C and supernatants were placed on a 96-well plate (round bottom). Isolated beads, representing the phagosomal fraction, were washed with cold 2% (w/v) BSA/PBS by centrifugation at 1,000 g during 5 min at 4°C and fixed with 1% (w/v) PFA/PBS during 10 min on ice. After two washes with 0.2 M glycine and one wash with 2% (w/v) BSA/PBS, samples were labeled ON at 4°C with the 25.D1 antibody coupled to APC or a combination of rabbit anti-OVA and rat anti-Lamp1 antibodies in 2% (w/v) BSA/PBS. When needed, samples were incubated with the secondary antibodies for 45 min at 4°C. Finally, stained phagosomal preparations were analyzed after gating on a particular FSC/SSC region corresponding to single beads in solution.

For antigen uptake assays, WT and GRASP55^{−/−} BMDCs were incubated for 1 h at 37°C with 0.1 or 0.3 mg/mL of soluble OVA conjugated to Alexa 647 in complete medium. The incubation at 4°C with the highest concentration of OVA-A647 was performed as a negative control for endocytosis. Then, cells were washed with 0.5% (w/v) BSA/PBS and the MFI was calculated by FACS analysis. To determine the phagocytic capacity of WT and GRASP55^{−/−} BMDCs, they were incubated with different amounts of 3-µm latex beads coated with OVA-A647 in complete medium during 1 h at 37°C or the highest dilution at 4°C. After this period, cells were extensively washed with 0.5% (w/v) BSA/PBS, labeled first with anti-OVA and then with a secondary anti-rabbit conjugated to Alexa 488. Finally, BMDCs were analyzed by flow cytometry, and the percentage of cells with beads fully internalized was determined.

All FACS experiments were done with a BD LSR II Flow Cytometer (BD Biosciences) equipment, and the analyses were performed by using the FlowJo Software.

Phagosome purification

WT and *GRASP55^{-/-}* BMDCs were incubated with 3-μm magnetic beads for 20 min at 18°C and 15 min at 37°C in free-serum IMDM medium (pulse). After washing with cold 2% (w/v) BSA/PBS, cells were incubated with rmGM-CSF-containing medium at 37°C to complete 1, 3 and 5 h of chase. BMDCs were disrupted with a syringe (22G needle) in homogenization buffer (PBS 8% sucrose, 3 mM imidazole, 1 mM DTT and 1X protease inhibitor cocktail), and phagosomes were removed from the post-nuclear supernatant using a magnet. After washing three times in cold PBS, phagosomal content was recovered by incubating the samples in lysis buffer (50 mM Tris-HCl pH 7.4, 0.5% NP-40 and 1X protease inhibitor cocktail) during 30 min at 4°C. Finally, cellular debris were excluded from the solution by centrifugation 5 min at 15,000 rpm, and protein concentration was determined by Bradford.

Exogenous antigen presentation

For Graspin-related experiments WT BMDCs were incubated for 5 h with 3 or 6 mg/mL of soluble OVA, or with OVA-coated 3-μm latex beads, or during 2 h with the indicated doses of SIINFEKL or ISQAVHAAHAEINEAGR peptides at 37°C. For all antigens, cells were treated (or not) with 50 μM of Graspin for 5 h. In the conditions involving the short peptides, a 3 h pre-incubation with Graspin was done before adding the peptides. Alternatively, JAWS-II DCs were incubated for 5 h with 0.5 or 5 mg/mL of soluble OVA, or with different ratios of OVA/BSA-coated 3-μm latex beads, or during 2 h with the indicated doses of SIINFEKL at 37°C. Cells were treated (or not) with 15, 30, or 60 μM of Graspin for a total time of 5 h. Then, BMDCs or JAWS-II DCs were washed with 0.5% (w/v) BSA/PBS, fixed with 0.008% glutaraldehyde during 3 min at 4°C, and quenched with 0.2 M glycine. After one final wash with PBS, B3Z or OT-IIZ T cells were added for 16 h at 37°C. T cell activation was measured by detecting β-galactosidase activity by optical density (absorbance at 595–655 nm) using CPRG as the substrate for the reaction.

Also, WT and *GRASP55^{-/-}* BMDCs were incubated for 5 h with 3 or 6 mg/mL of soluble OVA, or with OVA-coated 3-μm latex beads, or during 2 h with the indicated doses of SIINFEKL or ISQAVHAAHAEINEAGR peptides at 37°C. For all antigen presentation experiments in presence of LPS, BMDCs were treated for 12 h with 100 ng/mL of ultrapure LPS and then incubated for 5 h with 2 mg/mL of soluble OVA (Low Endo), or with OVA-coated 3-μm latex beads (Low Endo, OVA 10 mg/mL) at 37°C. For *T. gondii* presentation experiments, WT and *GRASP55^{-/-}* BMDCs were infected with TgRH GRA6-OVA or TgRH YFP SAG1-OVA parasites for 12 h at 37°C at the indicated multiplicity of infection (MOI). For *E. coli* presentation experiments, WT and *GRASP55^{-/-}* BMDCs were incubated with the *E. coli* DH5α-expressing OVA strain (at MOI 20) for 12 h at 37°C. Before this, the bacteria was incubated with 0.2 mM of IPTG to induce OVA expression. Finally, BMDCs were washed, fixed and confronted to B3Z or OT-IIZ T cells to evaluate their activation colorimetrically, as detailed before. Alternatively, total splenic DCs were recovered from WT and *GRASP55^{-/-}* mice using CD11c MicroBeads following the supplier's instructions. Then, CD11c+ cells were incubated with the different antigens (soluble OVA, OVA-coated 3-μm latex beads, SIINFEKL or ISQAVHAAHAEINEAGR OVA peptides) and exposed to B3Z or OT-IIZ cells to assess T cell activation, as described above.

For *in vivo* antigen presentation experiments, WT and *GRASP55^{-/-}* bone marrow chimeras were generated. B6/SJL mice, expressing the CD45.1+ congenic marker, were lethally irradiated (12 Gy) and were reconstituted intravenously with 5 × 10⁶ bone marrow cells from WT or *GRASP55^{-/-}* expressing CD45.2+ congenic marker. Mice were used 45 days after reconstitution. As the source of exogenous antigen, we used RAW 264.7 macrophages infected with recombinant vaccinia virus (VACV) expressing full-length OVA (VACV-OVA), a gift from Jonathan W. Yewdell and Jack R. Bennink (National Institutes of Health, USA) that was kindly provided by Margarita del Val (Centro de Biología Molecular Severo Ochoa, Spain). For this, VACV-OVA stocks were grown in CV-1 cell monolayers, titrated with crystal violet solution (0.5% crystal violet, 10% ethanol and 1% PFA), and used as clarified sonicated cell extracts. RAW 264.7 macrophages were cultured in DMEM supplemented with 10% heat-inactivated FBS, 100 μM non-essential amino acids (Thermo Fisher Scientific), 1 mM pyruvate, 2 mM L-glutamine, 100 U/mL penicillin, 100 μg/mL streptomycin (all four from Lonza), 10 mM HEPES (Sigma-Aldrich), and 50 μM 2-mercaptoethanol (Merck), herein called complete DMEM in 150 mm tissue culture treated dish. RAW 264.7 cells were infected with VACV-OVA at MOI 2 for 4 h and irradiated with Ultraviolet-C (240 mJ/cm²). Cell preparations were used 16 h later. Then, 2 × 10⁵ VACV-OVA-infected RAW cells were injected intraperitoneally in the chimeras. After 7 days, spleens were collected and incubated for 15 min with 250 μg/mL Liberase TL and 200 μg/mL DNase I (both from Sigma-Aldrich) in Hanks Balanced Salt Solution (HBSS) with 10 mM HEPES. After neutralization with heat-inactivated FBS, cells were smashed through 70 μm cell strainers and spun down at 1700 rpm for 5 min at 4°C. Splenic cell pellets were incubated with RBC Lysis Buffer (Sigma-Aldrich) for 3 min at RT, then neutralized with PBS supplemented with 2% FBS and 2 mM EDTA (FACS media) and spun down at 1700 rpm for 5 min at 4°C. One-tenth of the cells were stained for flow cytometry to analyze B8R⁺ cells, another tenth was cultured for 2 h in the presence of 1 μM 20–27 B8R peptide and a third tenth was cultured ON in the presence of 10 μM 262–276 and 60 μM 323–339 OVA peptides. After each culture, 5 μg/mL of Brefeldin A was added for 4 h, and cells were fixed and stained for flow cytometry.

For antigen presentation experiments of phagosomal fractions, WT and *GRASP55^{-/-}* BMDCs were incubated for 1 and 5 h (15 min pulse + 45 min or 4 h and 45 min chase) with OVA covalently coupled to 3-μm magnetic beads. After the chase periods, BMDCs were washed with cold 2% (w/v) BSA/PBS and disrupted with a syringe (22G needle) in homogenization buffer (PBS 8% sucrose, 3 mM imidazole, 1 mM DTT and 1X protease inhibitor cocktail). Then, phagosomes were removed from the post-nuclear supernatant by using a magnet, washed three times with cold PBS, fixed with 0.008% glutaraldehyde during 3 min at 4°C, and quenched with 0.2 M glycine. After one final wash with cold PBS, purified phagosomes were disrupted with an insulin syringe/needle so the MHC-OVA loaded molecules are freely exposed. Finally, these phagosomal membrane-enriched fractions were confronted to B3Z or OT-IIZ

T cells for 16 h at 37°C, and their activation was measured by adding CPRG. As a control, non-phagocytosed 3- μ m OVA-coated magnetic beads were incubated with B3Z or OT-IIZ cells to evaluate any potential nonspecific activation of CD8 $^{+}$ and CD4 $^{+}$ T cells by these particles.

Endogenous MHC-I antigen presentation

Soluble OVA was electroporated into BMDCs to measure direct MHC-I presentation, as we have previously described.²⁶ Briefly, WT and GRASP55 $^{-/-}$ BMDCs were pre-treated or not with 5 μ g/mL of Brefeldin A for 30 min at 37°C. After this time, BMDCs were extensively washed with PBS, suspended in 1 mM HEPES/PBS pH 7.4 + OVA at 3 mg/mL, and electroporated by using a Bio-Rad Gene Pulser II Porator (0.45 kV and 250 μ F of voltage and capacitance, respectively) to introduce OVA into the cytosol. Cells were immediately washed with cold PBS, resuspended in complete medium and incubated for 2 h at 37°C in the presence or absence of 5 μ g/mL Brefeldin A. Finally, BMDCs were washed, fixed with glutaraldehyde and confronted to B3Z T cells, as described before for exogenous antigen presentation experiments. CD8 $^{+}$ T cell activation was determined by quantifying β -galactosidase activity (optical density at 595–655 nm absorbance).

Immunofluorescence and microscopy

For confocal microscopy experiments, WT and GRASP55 $^{-/-}$ BMDCs were placed on poly-L-lysine-coated glass coverslips for 30 min at room temperature (RT). After one wash with PBS, cells were incubated in complete IMDM rmGM-CSF-containing medium for 1 h at 37°C in an atmosphere of 5% CO₂. BMDCs were washed with PBS, fixed with 2% (w/v) PFA/PBS for 15 min at 37°C and then quenched with 0.2 M glycine. After this, cells were permeabilized with PBS/0.05% saponin/0.2% BSA for 20 min at RT, washed, and incubated with the primary antibodies indicated for each figure ON at 4°C. The next day, cells were washed with permeabilization buffer and incubated with the secondary antibodies for 45 min at 4°C. Cells were washed again three times with permeabilization buffer and twice with PBS. For Figure 5B, BMDCs were incubated with OVA-coated 3- μ m latex beads for 5 h at 37°C after adherence to the coverslips. After the fixation and permeabilization steps, cells were stained with anti-Lamp1, anti-GRASP55, and anti-SIINFEKL peptide bound to H-2K b (25.D1) antibodies. For Figure S5A, BMDCs were incubated OVA-coated 3- μ m magnetic beads for 5 h at 37°C, fixed, permeabilized and stained sequentially with the anti-OVA and anti-rabbit A555 antibodies. Cells were washed three times with PBS/0.05% saponin/0.2% BSA, and incubated with 60 nM of phalloidin coupled to Alexa 488 diluted in PBS for 1 h at 37°C. For *T. gondii* infection experiments, WT BMDCs were infected with TgRH YFP SAG1-OVA parasites for 12 h at 37°C, placed on poly-L-lysine-coated glass coverslips, fixed, permeabilized, and stained with anti-GRA2 and anti-GRASP55 antibodies. For *E. coli* infection experiments, WT BMDCs were incubated with pHrodo Green *E. Coli* BioParticles for 12 h at 37°C, placed on poly-L-lysine-coated glass coverslips, fixed, permeabilized, and stained with anti-GRASP55. For all conditions, after secondary antibody staining, BMDCs were extensively washed with PBS, added 1 μ g/mL DAPI, washed again with PBS, and coverslips were mounted with FluorSave Reagent (Merck). Image acquisition was performed on a Leica SP8 confocal microscope with a 63x/1.4 NA oil immersion objective. One z stack plane is shown from the acquired images and they were processed with the ImageJ software (Wayne Rasband, National Institutes of Health). Image deconvolution was performed with the Parallel Iterative Deconvolution plugin (Piotr Wendykier) using a theoretical PSF generated by the Diffraction PSF 3D plugin (Robert Dougherty).

For STED microscopy experiments, WT BMDCs were infected with TgRH GRA6-OVA parasites for 12 h at 37°C and placed on poly-L-lysine-coated glass coverslips. Cells were fixed with 2% (w/v) PFA/PBS 10 min at 4°C and then permeabilized with 0.1% Triton X-100 also 10 min at 4°C. BMDCs were stained with anti-GRA2 and anti-GRASP55 antibodies ON at 4°C, extensively washed with PBS, incubated with fluorescent secondary antibodies 1 h at RT, and washed again with PBS. Finally, coverslips were carefully dried and mounted with Mowiol medium. Image acquisition was performed on a Confocal SP8-STED 3X microscope with a 100x/1.4 NA objective. One z stack plane is shown from the acquired images and they were processed with the ImageJ software.

QUANTIFICATION AND STATISTICAL ANALYSIS

Statistical analysis

The two-tailed Student's unpaired t test and the two-way ANOVA with Bonferroni post-test were performed at the indicated figures. Mean values, SEM and statistics were calculated by using the GraphPad Prism 5 software. We estimated the population mean because our study focused on the average value of the population, not on individual values. When comparing multiple means across different groups, using SEM provides a clearer indication of how precisely each mean is estimated. Results with a *p* value less than 0.05 were considered significant. All *p* values and sample size (*n*, number of replicates and independent experiments) are specified in every figure legend. No criteria of inclusion or exclusion of data were used in this study.